JGR Solid Earth

RESEARCH ARTICLE
10.1029/2023JB028405

Induced Polarization of Clayey Rocks and Soils: Non-Linear Complex Conductivity Models

Youzheng Qi[1] and **Yuxin Wu**[1]

[1]Earth and Environmental Sciences Area, Lawrence Berkeley National Laboratory, Berkeley, CA, USA

Abstract The past decades have witnessed the increased applications of induced polarization (IP) method in the critical zone studies with ubiquitous clay minerals. Although IP outperforms traditional electrical and electromagnetic methods through its unique ability to measure quadrature conductivity, the nonlinearity that quadrature conductivity behaves with salinities and frequencies greatly tortures IP practitioners, as (a) salinity-dependency makes the quadrature conductivity a varyingly unstable parameter to quantitatively estimate hydraulic properties and clay content; (b) frequency-dependent Cole-Cole and Debye/Warburg decomposition models, although mathematically sound, physically mingle the properties of pore water and clay minerals and are empirical in nature. From basic principles, we demonstrate that quadrature conductivity remains a hybrid property involving both clay and water, and develop relevant models to distinguish them. Our models are validated by theories, experiments, simulations, and comparisons, all of which proclaim considerable advantages over previous models and offer the prospect of quantitative applications.

Plain Language Summary As habitually appears in the first chapter of many geophysics textbooks, rock and soil models (i.e., petrophysics) lay the base for geophysical applications, bridging the gap between macro-scale field and micro-scale rock/soil parameters such as porosity and permeability. In contrast to "clean" rocks and soils where Archie's law is readily used, the additional interfacial conduction and polarization arising from the electrical double layer of "dirty" rocks and soils, especially clayey ones, greatly complicate this issue and bring both challenges and opportunities. On the one hand, this interfacial conduction nullifies Archie's law, making the porosity evaluation challenging, but, on the other hand, these interfacial properties provide an opportunity to assess the pore structure and clay properties, making the permeability estimation possible. Although IP is highly commendable to separate the interfacial attribution from the bulk water, complex conductivity models that can both physically and mathematically explain clayey rock/soil behaviors are lacking, which is the goal of our work. We expect our developed models to deepen the understanding of IP mechanisms and lead to more quantitative IP applications.

Key Points:

- Salinity- and frequency-dependent nonlinearities lie at the crux of induced polarization mechanisms
- Quadrature conductivity increases with salinity mainly by virtue of the coupling between electrical double layer (EDL) and water
- Frequency dependency of clayey rocks and soils stems from the leaky-capacitor behavior of the EDL

Supporting Information:

Supporting Information may be found in the online version of this article.

Correspondence to:

Y. Qi and Y. Wu,
YouzhengQi@lbl.gov;
YWu3@lbl.gov

Citation:

Qi, Y., & Wu, Y. (2024). Induced polarization of clayey rocks and soils: Non-linear complex conductivity models. *Journal of Geophysical Research: Solid Earth*, *129*, e2023JB028405. https://doi.org/10.1029/2023JB028405

Received 28 NOV 2023
Accepted 7 MAR 2024

Author Contributions:

Conceptualization: Youzheng Qi, Yuxin Wu
Methodology: Youzheng Qi
Supervision: Yuxin Wu
Validation: Youzheng Qi, Yuxin Wu
Writing – original draft: Youzheng Qi
Writing – review & editing: Yuxin Wu

1. Introduction

It has been beyond 100 years since the first IP work was pioneered by Conrad Schlumberger in the 1910s (Schlumberger, 1920; Seigel et al., 2007), during which the IP community evolved from the initial mineral exploration into much broader areas such as hydrological, biological, environmental, and engineering investigations (Binley & Slater, 2020; Kemna et al., 2012; Kessouri et al., 2019; Loiseau et al., 2023; Luo & Zhang, 1998; Rubin & Hubbard, 2006; Wu et al., 2010). In the multidisciplinary and multiscale critical zone studies, IP is surging due to its specialties over traditional electrical and electromagnetic (E&EM) methods (Parsekian et al., 2015; Robinson et al., 2008). E&EM methods measure how energy is lost in geomaterials, while IP method also senses how energy is stored (Sumner, 1976). It is widely recognized that this energy storage is implemented by the electrical double layers (EDLs) that exist at the interfaces between geomaterials and their interstitial fluids (Winsauer & McCardell, 1953). For some geomaterials like sands and gravels, E&EM energy mostly dissipates via the volume conduction within the pore water, such that the conventional E&EM methods and the well-known Archie's law are readily used (Archie, 1942). However, for some geomaterials, especially the omnipresent clayey rocks and soils in Earth's near-surface (Schroeder, 2018), their high surface area and net negative surface charges make their EDLs rather forceful (Tournassat et al., 2015), such that the energy loss (i.e., conduction) and storage (i.e., polarization) resulting from the interfacial EDL are not inconsiderable anymore (Tabbagh et al., 2021), where established E&EM methods and related petrophysical models begin to fall short of expectations (Schön, 2015). By contrast, with the aforementioned unique ability, IP can not only separate the volume and surface contributions to estimate the true formation factor and clay content (Slater & Lesmes, 2002;

Weller et al., 2013), but also obtain the pore geometry information to assess permeability (Börner et al., 1996; Rink & Schopper, 1974), the Holy Grail of hydrogeology, both of which are beyond the competence of E&EM methods (Binley et al., 2015; Slater, 2007).

Despite the obvious advantages, IP faces huge challenges of establishing itself as a routine method since its parameters, for example, quadrature conductivity σ'', surface conductivity σ_s, and normalized chargeability Mn, vary in an unstable way with their causal physical properties, for example, the surface area per pore volume S_{por} (Lévy et al., 2019; Weller & Slater, 2019), such variance not being explained by current models (Peshtani et al., 2022). Given that these parameters are extracted from multi-salinity and/or multi-frequency measurements, salinity- and frequency-dependent responses lie at the root of IP model development. Unfortunately, these two behaviors are highly non-linear and there is a long-standing debate over their underlying mechanisms. Regarding the salinity-dependent nonlinearity, some believe it results from the variable EDL properties (Börner, 1992; Revil & Skold, 2011), while others ascribe this mainly to the rock/soil geometry (Niu, Revil, & Saidian, 2016; Revil et al., 2019). The former group employ Waxman-type models (Vinegar & Waxman, 1984; Waxman & Smits, 1968), while the latter use Bruggeman-Hanai-Sen (BHS) model (Sen et al., 1981), two models differing from each other mathematically and physically (Bussian, 1983; de Lima & Sharma, 1990; Niwas et al., 2006, 2007). Recently, Qi and Wu (2022) presents a new model that integrates Archie's law and a composite surface conductivity to account for such a nonlinearity. Although that model is comparable with the well-established BHS model, it is developed conceptually and with applications to real electrical conductivity for E&EM rather than complex electrical conductivity for IP. Meanwhile, as to the frequency-dependent nonlinearity, it is understood this stems from the EDL's leaky-capacitor behavior, yet those to depict such low-frequency dispersion are Cole-Cole and Debye/Warburg decomposition models (Nordsiek & Weller, 2008; Pelton et al., 1978) that originally characterize high-frequency dielectric relaxations. Although mathematically works for IP, physically these models mingle the surface and bulk attributions and are essentially empirical models (Weigand & Kemna, 2016b).

There is a pressing need for models that can both physically and mathematically account for these two nonlinearities, as this directly relates to how electrochemical properties are assembled into mechanistic models and different models supply distinct petrophysical parameters to geophysicists both in laboratory and field (Cosenza et al., 2009; Glover, 2015). To this end, we return to the basic principles behind these phenomena: electrochemistry and Maxwell's equations, from which we pinpoint that both surface and quadrature conductivities are mixed properties following the same EDL-and-water pattern and thence develop related non-linear models. Theories, simulations, measurements, and comparisons all corroborate our models and exhibit their advantages over existing models. It is expected that our models could shed new light on the IP mechanism and pave the way for more quantitative IP applications.

2. Model Development and Verification

2.1. Underlying Principles

IP method can be seen as an extension of DC resistivity method where frequency- or time-domain signals are transmitted into earth and corresponding responses are measured. In view of the Fourier-transform equivalence (Fiandaca et al., 2012; Qi et al., 2019), IP models are always developed in frequency domain, namely spectral IP (SIP). Figure 1 give typical conductivity curves of clayey rocks/soils at a certain frequency. Compared to ideally "clean" rocks/soils, two distinctive features emerge (Mendieta et al., 2021; Weller, Zhang, & Slater, 2015): (a) The real conductivity is no longer a straight line across the origin but bears an excess surface conductivity σ_s that behaves non-linearly at low/medium salinities but appears constant at high salinities. (b) It has an additional term of quadrature conductivity σ'' that is also non-linear at low salinity, but seems to flatten at medium salinities and then decrease at high salinities. It is straightforward that these nonlinearities result from EDLs, otherwise it will be an Archie-type straight line and has no quadrature term for clean rocks/soils (Archie, 1942), where the bulk pore water is approximately the only conductive phase. It shall be clarified here that "cleanness" or "dirtiness" is a relative terminology that is essentially a question about the ratio between the effective EDL and pore water conductivity (i.e., the Dukhin number. cf., Lyklema, 2002). These nonlinearities may not be a big issue for near-clean geomaterials, but, by contrast, they are obviously significant for those dirty clayey rocks/soils (Schön, 2015), which makes things a bit complicated and more theoretical works are clearly needed.

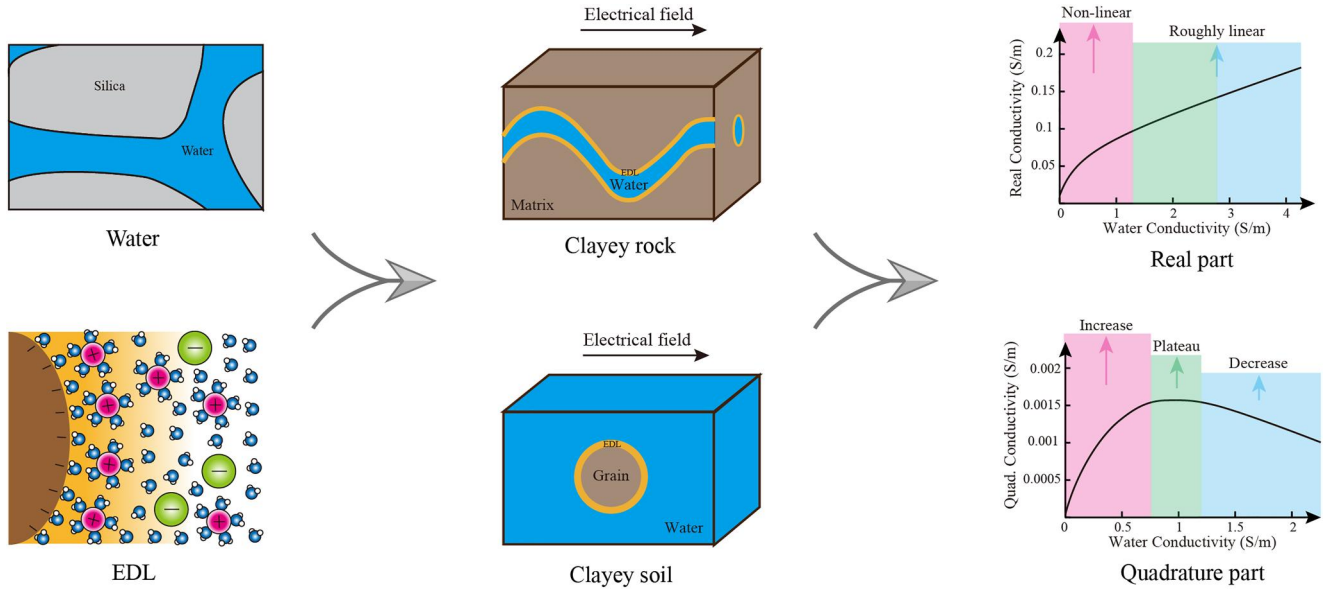

Figure 1. Mechanistic model-developing diagram includes the assembly of bulk water and EDL properties (leftmost) into an effective medium model (middle) that finally produces non-linear complex-conductivity curves (rightmost).

As from the model-developing diagram of Figure 1 (Jougnot et al., 2010; Leroy & Revil, 2009), these features result merely from two aspects: EDL properties and effective medium models, as water itself is non-polarizable for SIP of 1mHz-1 kHz (Revil et al., 2023; Vinegar & Waxman, 1984). Indeed, an enduring debate does exist between these two sources: some believe this is from EDL variation (Börner, 1992; Revil & Skold, 2011), while others argue this is mainly from the rock/soil geometry (Bussian, 1983; Johnson & Sen, 1988). Put aside the quadrature decrease at high salinities and focus on the non-linear increase first. Diffuse layer polarization (DLP) model (Börner, 1992) cannot even mathematically explain the non-linear increase (Weller & Slater, 2012), thus is easily excluded. Stern layer polarization (SLP) model (Skold et al., 2011) does cause a concave nonlinearity, but this merely happens at extremely low salinity (e.g., <0.05 S/m) and cannot explain such a strong nonlinearity (Bernabé & Revil, 1995; Niu, Revil, & Saidian, 2016), which means that SLP model may mathematically explain measurements, but it can generate physically unreasonable parameter correlations (Weller, Zhang, & Slater, 2015). Considering EDL variation reasoning is arguable, from Figure 1, effective medium model is the only remaining cause.

As geophysical methods work in macro-scale that have sensitivity but limited resolution into micro-scale, effective medium models are generally utilized to bridge the gap between micro- and macro-scales and to produce useful parameters for the composite geomaterials. Although effective medium theory (EMT) inevitably simplifies the geometry so that analytic formulas can be developed for real-world geomaterials, it solidly builds on the underlying principle of Maxwell's equations. A vivid example of effective medium models is Archie's law (Archie, 1942) that has been successfully used for more than 80 years for “clean” rocks/soils. Regarding “dirty” ones, Figure 1 shows simplified models that mimic the geometry of consolidated rocks and unconsolidated soils where EDL clings along the pore wall and grain surface, respectively. Given the fact that EDL size (salinity-dependent yet typical <40 Å) is mostly smaller than the typical pore size (>1,000 Å) (Johnson et al., 1986), the specific EDL conductivity Σ_s^* performs as a 2D model without thickness in the unit of S rather than S/m (Dukhin & Derjaguin, 1974; Lyklema, 1995) as

$$\Sigma_s^* = BQ_s + i\lambda Q_s, \tag{1}$$

where Q_s is the charge density per unit surface, B and λ the apparent mobilities for conduction and polarization, respectively. Here Σ_s^* is complex-valued because EDL performs as a leaky capacitor under E&EM field, both conducting and storing energies (Lyklema et al., 1983; Schwarz, 1962). Note that for tight rocks, EDL can be comparable in size to the pore that leads to phenomena such as EDL interaction. To make Equation 1 applicable, this can be overcome with equivalent potential approaches such as Donnan equilibrium (Jougnot et al., 2009).

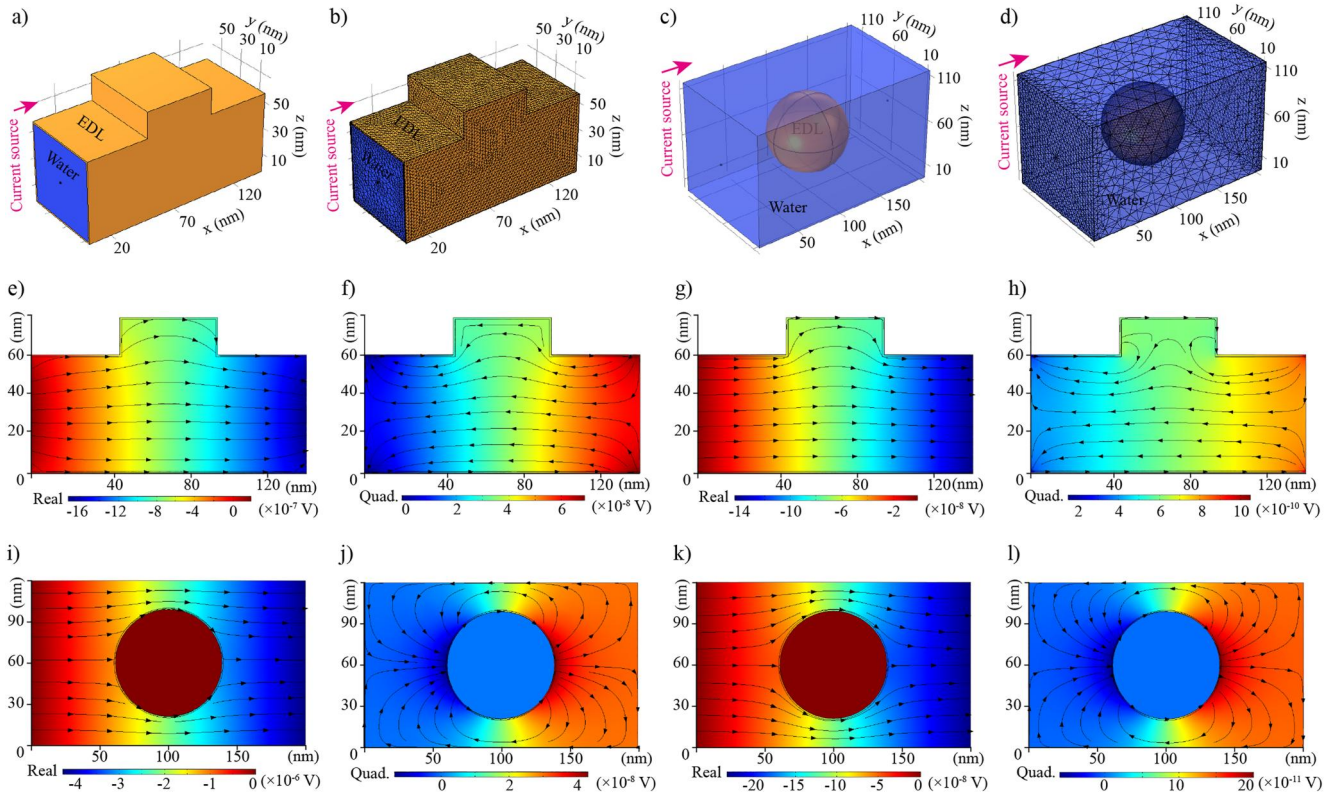

Figure 2. Simulations testify to the root cause of the salinity-dependent nonlinearity. Panels (a, b) and (c, d) are geometry and meshes for pore-scale rocks and grain-scale soils, respectively. Panels (e–h) and (i–l) are the simulated potential V and current I distributions for rocks and soils at low- (0.05 S/m) and high-salinity (1 S/m), respectively. Note that V (in color scales) and I (in black arrowed lines) bear the same information since they are perpendicular to each other.

If we hypothesize that (a) There is no E&EM coupling between EDL and pore water, such that they perform as two paralleled circuits; (b) There is a bodiless electrode connecting to the EDL during measurements, the bulk conductivity σ^* shall be a linear circuit model as (Dukhin et al., 2012)

$$\begin{aligned}\sigma^* &= \frac{\sigma_w}{F} + \sigma_c^* \\ &= \frac{\sigma_w}{F} + \frac{2\Sigma_s^*}{\Lambda} \\ &= \frac{\sigma_w}{F} + \Sigma_s^* S_{por} \\ &= \frac{\sigma_w}{F} + (B + i\lambda) Q_v\end{aligned}, \tag{2}$$

where the first term is Archie's law with $F = \phi^{-m}$ the intrinsic formation factor, ϕ porosity and m the cementation exponent (Archie, 1942). $\sigma_c^* = 2\Sigma_s^*/\Lambda$ denotes the equivalent volume conductivity of the solid phase (i.e., Effective EDL conductivity) since an insulating sphere coated with a non-thick 2D surface conductivity Σ_s^* behaves just as a 3D sphere with uniform conductivity $2\Sigma_s^*/\Lambda$ (O'Konski, 1960; Schurr, 1964), where Λ is the radius of the sphere and, for natural rocks/soils, Λ can be linked to the characteristic pore or grain size (Johnson et al., 1986). $S_{por} = 2/\Lambda$ is the surface area per unit pore volume and $Q_v = Q_s S_{por}$ is the ionic concentration per unit pore volume.

Unfortunately, the aforementioned hypotheses never exist in the real world because (a) There is a direct coupling between EDL and water, such that the existence of EDL will disturb the field in the water and vice versa (Dukhin & Derjaguin, 1974); (b) There is no immaterial electrode and SIP electrodes are much bigger than EDL. Indeed, in the IP realm, (a) is exploited to fulfill (b); that is, electrodes are put into water to measure the total field that

includes both the field of water conduction (background field) and the disturbed field from EDL (anomalous field). Because of this coupling, Kirchhoff's circuit laws cannot apply and Maxwell's equations, downscaled to Poisson's equation for SIP of 1mHz-1 kHz, must be used since clayey rocks/soils already behave as distributed elements rather than lumped parameter system (cf., Supporting Information S1).

Considering one can never keep EDL a hundred percent constant in experiments, simulation is the best way to validate whether this coupling can decisively cause the salinity-dependent nonlinearity or not (Niu & Zhang, 2017; Revil et al., 2018). As in Figures 2a–2d, for consolidated rock, one block ($140 \times 60 \times 60$ nm) and another small block ($50 \times 60 \times 20$ nm) are fused to imitate a dead end, around whose sides a 1 nm layer is built to represent EDL, while for unconsolidated soil, a block ($200 \times 120 \times 120$ nm) to represent the water cube and then implant one sphere (radius 40 nm) bearing a shell (1 nm) to mimic the clayey grain. Since we exclude EDL variation, EDL conductivity is set as $0.5 + 0.05i$ S/m (i.e., $\Sigma_s^* = 5 \times 10^{-10} + 5 \times 10^{-11} i$ S) and the water conductivity changes at 6 variables of [0.01, 0.1, 0.5, 1, 5, 10] S/m to model multi-salinity measurements. All outside faces are given insulating boundary conditions except two end-faces with current source/sink (± 1 A/m^2) and two points in its middle to resemble point-measuring electrodes (Jougnot et al., 2010). The governing equation is the frequency-domain Poisson's equation and the numerical method is the finite-element method. Simulated real and quadrature results are exemplified in Figures 2e–2l, conveying distinctive features that quadrature voltages act with the opposite sign to real voltages and such quadrature voltages not only distribute in EDLs but also in water, which may be surprising at first glance but is rather reasonable after contemplation. The quadrature voltage in the water, albeit non-polarizable by itself, is coupled by the polarized EDL. The fact remains that it is the real and quadrature voltages in the water that we measure in SIP. Finally, voltages are extracted at two points and calculated with currents and geometric factors to derive the simulated rock and soil conductivities in Figures 3a and 3d, respectively, which exhibit much the same non-linear increase as laboratory measurements. It stands to reason that the coupling between EDL and water (aka "the EDL-and-water pattern") gives rise to such salinity-dependent nonlinearity since in all cases EDL conductivity is set as a constant and, conceivably, salinity increase intensifies this EDL-and-water coupling, such ratiocination being in line with the precedents of Bussian (1983), Niwas et al. (2007), and Niu, Revil, and Saidian (2016) that also discover even constant EDLs still lead to the non-linear complex conductivity increase in the multi-salinity situation by the calculation of the well-established BHS model, where their geometry attribution carries the same meaning of the EDL-and-water coupling herein.

2.2. Non-Linear Salinity-Dependent Model

It is self-evident that the EDL-and-water coupling nullifies the linear model Equation 2 and non-linear model must be developed. Here we resort to the integral equation that is commonly used in the E&EM community (Christensen, 1997; Zhdanov & Fang, 1996)

$$\mathbf{E}(\mathbf{r}) = \mathbf{E}_w(\mathbf{r}) + \int \mathbf{G}\left(\mathbf{r},\mathbf{r}'\right) \cdot \left(\sigma_c^* - \sigma_w\right) \mathbf{E}\left(\mathbf{r}'\right) d\mathbf{r}', \tag{3}$$

where the total field $\mathbf{E}(\mathbf{r})$ are expressed as the background field $\mathbf{E}_w(\mathbf{r})$ and the anomalous field (the second term) where $\mathbf{G}(\mathbf{r}, \mathbf{r}')$ is the dyadic Green function and $\mathbf{r}$ and $\mathbf{r}'$ denote the coordinates of the background water and the anomaly of clay, respectively. σ_c^* bears the same expression as in Equation 2

$$\begin{aligned} \sigma_c^* &= (B + i\lambda) Q_v \\ &= (B + i\lambda) Q_s S_{por} \\ &= (B + i\lambda) Q_s \frac{2}{\Lambda} \end{aligned} \tag{4}$$

σ_c^* is verily what the 2D EDL (in comparison with the pore/grain, cf., Schwarz, 1962) represents itself in 3D since real-world measurements are all conducted in 3D. Considering the solid phase is insulating except for the surface, surface conduction $(B + i\lambda)Q_s$ is equivalent to the bulk conduction of $(B + i\lambda)Q_v$ under the relationship of $Q_v/Q_s = 2/\Lambda$, which is absolutely accurate for a spherical grain with the radius of Λ (O'Konski, 1960) or for a cylindrical capillary tube with the internal radius of Λ (Dukhin et al., 2012), but $2/\Lambda = S_{por}$ will become effective values for natural rocks and soils. Although σ_c^* is extensively used by many IP practitioners (e.g., Bussian, 1983;

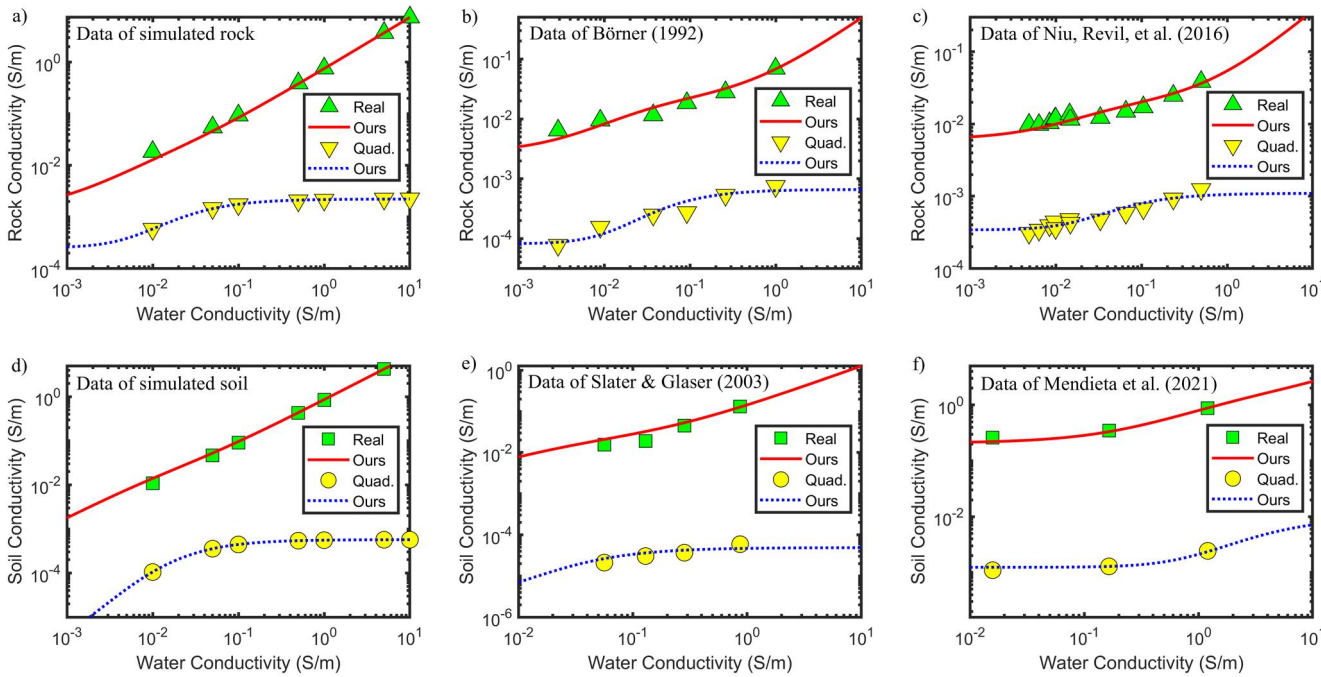

Figure 3. Our non-linear salinity-dependent model validation. Panels (a and d) are the simulated rock and soil at 1 Hz, while (b), (c), (e), and (f) are natural samples from sandstone E10 of Börner (1992) at 1 Hz, Portland sandstone PS1 of Niu, Revil, and Saidian (2016) at 100 Hz, sandy sediment N1-51-53 of Slater and Glaser (2003) at 1 Hz, and green montmorillonite MtG of Mendieta et al. (2021) at 1.46 Hz, respectively. For experimental data, salinities above 1 S/m are omitted because of obvious high-salinity decrease.

de Lima et al., 2005; Niu, Revil, & Saidian, 2016; Revil et al., 2019), it appears that there is not a universal name of σ_c^* in the nomenclature of IP. For lack of a better name, σ_c^* is dubbed as the effective EDL conductivity here.

From EMT, effective bulk conductivity of rocks and soils σ^* links to the total field $\mathbf{E}(\mathbf{r})$ via averaging the local electrical energy over the total volume V_{tot} as (Johnson et al., 1986)

$$\sigma^* = \frac{\int \sigma(\mathbf{r})|\mathbf{E}(\mathbf{r})|^2 dV_{tot}}{\int |\mathbf{E}(\mathbf{r})|^2 dV_{tot}}. \tag{5}$$

Unfortunately, although Equation 3 is directly from Maxwell's equations and thus absolutely accurate, it is hard to derive an explicit-form effective medium model because $\mathbf{E}(\mathbf{r})$ exists on both sides. Thanks to the much smaller size of EDL compared to the bulk, Born approximation can be readily employed to equal the total field in the EDL $\mathbf{E}(\mathbf{r}')$ by the background field $\mathbf{E}_w(\mathbf{r}')$ as (Christensen, 1997; Habashy et al., 1993)

$$\mathbf{E}(\mathbf{r}) = \mathbf{E}_w(\mathbf{r}) + \int \mathbf{G}\left(\mathbf{r},\mathbf{r}'\right)\cdot\left(\sigma_c^* - \sigma_w\right)\mathbf{E}_w\left(\mathbf{r}'\right)d\mathbf{r}'. \tag{6}$$

With that, integrating the right side with their respective local conductivity over the pore volume V_p and then averaging them to the total volume V_{tot} will derive the expression of effective bulk conductivity (Johnson et al., 1986), where the first term will be Archie's law (Niu, Prasad, et al., 2016)

$$\frac{\sigma_w}{F} = \frac{\int \sigma_w |\mathbf{E}_w(\mathbf{r})|^2 dV_p}{\int |\mathbf{E}_w(\mathbf{r})|^2 dV_{tot}}, \tag{7}$$

yet the second term, the so-called complex surface conductivity

Table 1
Petrophysical Properties of Tested Samples and Our Model-Fitted Parameters

Sample ID in Figure 3	Sample ID in literature	Consolidation type	Specification	Porosity ϕ (−)	S_{por} (μm^{-1})	F' (−) in literature	F (−)	ξ_w (%)	σ_c' (S/m)	σ_c'' (S/m)
3a	–	Rock	Simulation	–	–	–	1.3	48	0.003	0.0006
3b	E10	Rock	Sandstone	0.2238	41.6	17	21.4	46	0.0062	0.0002
3c	PS1	Rock	Portland sandstone	0.194	38.424	37.26	28.4	27	0.0095	0.0005
3d	–	Soil	Simulation	–	–	–	1.2	89	0.0005	2.3×10^{-5}
3e	N1 51-53	Soil	Sandy sediment	0.41	3.775	5.35	8	61	0.0033	8.6×10^{-6}
3f	MtG	Soil	Green montmorillonite	0.68	92.52	3.6	8	46	0.47	0.0028

Note. S_{por} of PS1, N1-51-53, and MtG shown here are calculated from their specific surface area per unit mass (S_m) via $S_{por} = S_m \rho_g (1-\phi)/\phi$ (Weller et al., 2010) with an assumed density of ρ_g = 2,650 kg/m^3.

$$\sigma_s^* = \frac{\int (\sigma_c^* - \sigma_w) |\mathbf{G}(\mathbf{r}, \mathbf{r}') \cdot \mathbf{E}_w(\mathbf{r}')|^2 dV_{sld}}{\int |\mathbf{E}_w(\mathbf{r})|^2 dV_{tot}}, \tag{8}$$

is too complicated to derive because analytic $\mathbf{G}(\mathbf{r}, \mathbf{r}')$ doesn't exist for natural clayey rocks/soils, albeit Equation 8 clearly presents itself as a composite parameter of σ_c^* and σ_w. Nonetheless, it is proved by Brown (1955) that Maxwell Garnett equation (Garnett, 1904) is statistically "the best" mixing rule for any two-phase mixture without knowing more than their respective fractions and properties, "the best" figuratively implying its simplicity yet broad applicability. Moreover, another specific advantage of the Maxwell Garnett equation that can be taken is that it is an asymmetric effective medium model where one phase must be chosen as the host (i.e., the matrix) and the other as the guest (i.e., the inclusion). From EMT, which phase is the host or guest depends on whose role is stronger or weaker rather than their respective fractions (Sihvola, 1999). As discussed in the preceding section, in clayey rocks/soils, water plays two roles: (a) Water conduction by itself; (b) Convey the complex field disturbed by EDL, while EDL plays one role: Being the source of the complex field in the pore water. It is obvious that water plays a stronger role than EDL in the bulk rock/soil conductivity σ^*, but, by contrast, in the complex surface conductivity σ_s^*, EDL plays a stronger role than water, as EDL is the source of σ_s^*, while σ_w just conveys the field, which implies that in σ_s^*, σ_c^* must be the host and σ_w the guest, with which we derive

$$\sigma^* = \frac{\sigma_w}{F} + \frac{(2\xi_w + 1)\sigma_c^* \sigma_w + 2(1-\xi_w)\sigma_c^{*2}}{(2+\xi_w)\sigma_c^* + (1-\xi_w)\sigma_w} \tag{9}$$

or

$$\sigma^* = \frac{\sigma_w}{F} + \frac{(3-2\xi_c)\sigma_c^* \sigma_w + 2\xi_c \sigma_c^{*2}}{(3-\xi_c)\sigma_c^* + \xi_c \sigma_w}, \tag{10}$$

where ξ_w and ξ_c are the apparent surface fraction of water and clay in such a clay-and-water pattern with $\xi_w + \xi_c = 1$. "Surface fraction" indicates this term provides a service for the surface rather than the bulk, while "apparent" implies they are effective values since they compensate for other geometrical features (Brown, 1965); that is, Equations 9/10 is not a hundred-percent reflection of a specified clayey rock/soil, but would be accurate to the second order (Brown, 1955). As an aside, Equation 9 is exactly the same as the model in Qi and Wu (2022) except that theirs is real-valued and developed conceptually, while here we abandon their schematic descriptions, impart theoretical pedigree to this model, and extend it into the complex domain for IP. Although Equations 9/10 resembles a similar form to two parallel circuits, it is stressed that they are indeed effective medium models derived from Maxwell's equations and have nothing to do with circuit laws. As evidenced in the simulations of Figure 2, there are no two separate conduction paths in rocks/soils and every field there is coupled as the total field in the pore water. Circuit laws not only cannot simulate this distributed pattern, but also cannot explain these

coupling phenomena, let alone develop effective medium models. In fact, most effective medium models, such as Archie's law (Archie, 1942), BHS (Sen et al., 1981), and Kozeny–Carman model (Carman, 1937), all bear this genre of simple formulas because simple geometries, such as spherical grains and capillary bundles, are normally employed in EMT. Although simple, effective medium models are of paramount importance to petrophysics because of their compactivity to reproduce the measured response with only a few effective parameters, from which petrophysical properties can be estimated.

To validate Equation 9, it is tested on both simulated and independently measured rocks and soils in Figure 3 with the model-fitted parameters in Table 1, where our model succeeds in capturing these non-linear conductivities with coefficient $R^2 > 0.97$. It is emphasized that here the used optimization algorithm is the complex-valued non-linear least-squares method where real and quadrature conductivities must be weighted to the same level (Weigand & Kemna, 2016a), otherwise one may find only the real part well-fitted. In Table 1, for the formation factor F, the simulated rock and soil have a rather low F just because rather simple geometries with very small solid phase are constructed in our simulated rock and soil, which is reasonable to deviate from real-world rocks and soils. An interesting phenomenon shown for those formation factors is that our F is mostly bigger than those F' in the literature except for Niu, Revil, and Saidian (2016). This is mainly because here we use the non-linear complex conductivity model of Equation 9, while those in the literature use the linear model (i.e., $\sigma = \sigma_w/F + \sigma_s$) that treats the surface conductivity σ_s as a constant. Such a difference strongly demonstrates the importance of employing a non-linear complex conductivity model because: (a) Using the linear equation with constant surface conductivity to model-fit the bulk conductivity of clayey samples tends to underestimate its formation factor F because data belonging to the non-linear portion are easily contained in such a linear model-fitting (Qi & Wu, 2022); (b) Using the linear model to obtain F means neglecting quadrature conductivity. It is known that real and quadrature parts of a complex function follow the Kramers–Kronig relation (i.e., Hilbert transform) (Pelton et al., 1983; Shuey & Johnson, 1973), and thus neglecting quadrature part means abandoning valuable information therein. As to the bigger F' from the BHS model employed by Niu, Revil, and Saidian (2016), it should result from the intrinsic difference of the cementation exponent m between Archie's law and BHS model (de Lima et al., 2005). Assuming an Archie's cementation factor of $m = 2$ for the sandstone would derive a formation factor of 26.6 which is in line with our value of 28.4.

Regarding those ξ_w values in Table 1, they are rather stable between 0% and 100% during our model-fitting. Given the fact that σ_s^* is definitely a composite parameter between σ_c^* and σ_w in physics, it is with ease that ξ_w never reach 0 or 1 in applications. It is underlined that ξ_w is a servant factor for surface properties that distinguishes the contributions between σ_c^* and σ_w, which is labeled as surface fraction and should not be confused with the volume fraction of bulk water, the latter being contained in F rather than σ_s^*. As to σ_c^*, from Equation 4, it holds a linear relationship with Q_v and such a linear relationship should cross the origin of coordinates. Although Q_v may be roughly estimated from S_{por} through a presumed Q_s, unfortunately, these S_{por} values here are all measured by nitrogen adsorption Brunauer-Emmett-Teller (BET) method that is rough for illite and especially unacceptable for smectite clays because of its inability to sense interlayers (Tournassat et al., 2013; Weller, Slater, et al., 2015). Thus, instead of testing such a linear causal relationship here, it will be validated on another independently measured data from Waxman and Smits (1968) in the following section where our model is compared with other models, For the data of Waxman and Smits (1968), wet-state titration method is employed to acquire Q_v in a more reliable way where our model does output a pretty good linear causal relationship that is consistent with the well-established BHS model.

Despite the good performance, Equations 9/10 cannot explain the high-salinity decrease of quadrature conductivity but predicts a high-salinity plateau. Similar to the increase, this decrease sparks widespread debate that argues membrane polarization (Hördt et al., 2016), ionic mobility (Lesmes & Frye, 2001), or clay aggregation (Mendieta et al., 2021) may be the cause. Since our work here focuses on the critical zone under freshwater conditions, we exclude this phenomenon in our model and appraise this as an open question for the community.

2.3. Non-Linear Frequency-Dependent Model

Besides the salinity-dependent nonlinearity, clayey rocks/soils manifest strong frequency-dependent nonlinearity (Mendieta et al., 2021; Niu, Revil, & Saidian, 2016; cf., Figure 4). In contrast to the former, there is a consensus that the latter results from the leaky-capacitor behavior of EDLs whose ions move backwards and forwards around rock pores and soil grains under multi-frequency field which usually causes a peak in the quadrature

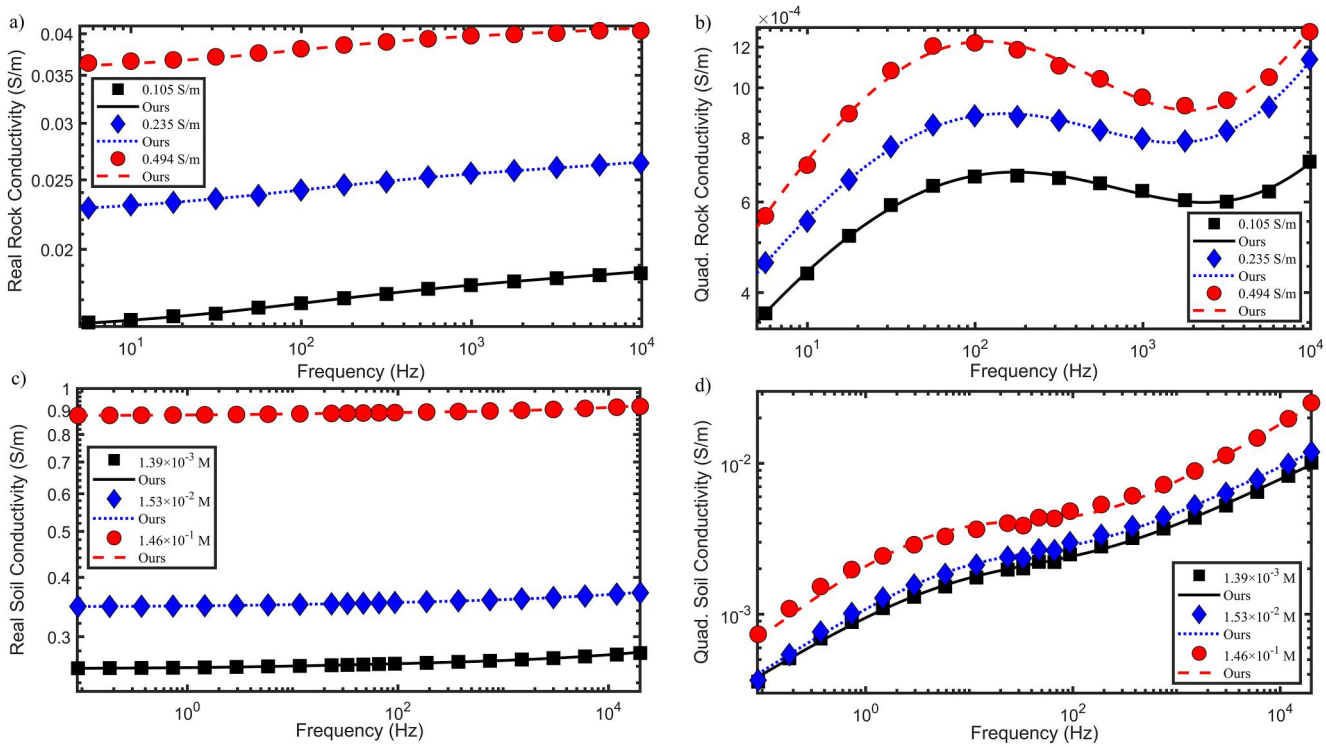

Figure 4. Our non-linear frequency-dependent model validation. Panels (a, b) and (c, d) are complex conductivities of the Portland sandstone PS1 of Niu, Revil, and Saidian (2016) and the green montmorillonite MtG of Mendieta et al. (2021), respectively. Note that extremely low- and high-frequency data are omitted because of their strong artifacts.

conductivity at one critical frequency (Lyklema et al., 1983; Schwarz, 1962). Considering this low-frequency EDL polarization is, albeit physically distinct, mathematically similar to the high-frequency dielectric polarization, models from the latter can be smoothly introduced to the former, meaning that we can use Debye/Warburg decomposition or, the most popular, Cole-Cole model to parameterize Σ_s^* or σ_c^* (Leroy & Revil, 2009; Leroy et al., 2008). However, it is found these models can not only describe the micro-scale EDL, but also the macro-scale clayey rocks/soils (Tarasov & Titov, 2013; Weller & Slater, 2022), which is quite surprising because all said models are developed from circuit laws that is justifiable for micro-scale dielectrics (e.g., molecules) and EDLs that have much smaller size than the excitation field, thus behaving as resistor-capacitor elements all by themselves, while macro-scale clayey rocks/soils are evidently distributed parameter systems (cf., Supporting Information S1). Thanks to Soininen (1984) and Luo and Zhang (1998) that unravel this paradox with the proof that the response of a Cole-Cole anomaly in an unpolarizable background still performs like a Cole-Cole model. That means, the occurrence that rocks and soils behave as a Cole-Cole model results from the fact that their EDLs themselves perform in the Cole-Cole way. In point of fact, this attribution is underpinned by the colloid science community where Schwarz (1962) and Lyklema et al. (1983) theoretically prove that the EDL of a spherical colloid displays a Debye-type polarization under low-frequency electric field. With the distribution of counterion activation energies in the EDL and the distribution of grain sizes, those colloidal EDLs will disperse to perform as a Cole-Cole model in practice (Lyklema et al., 1986; Schwarz, 1962).

Although Cole-Cole model

$$\sigma^* = \sigma^\infty + \frac{\sigma^0 - \sigma^\infty}{1 + (i\omega\tau)^c}, \tag{11}$$

where σ^0 and σ^∞ are the low- and high-frequency asymptotic conductivities, respectively, τ the characteristic relaxation time and c the Cole-Cole exponent, can describe clayey rocks/soils mathematically, physically it has the drawback of mingling bulk and surface properties together, σ^0 and σ^∞ including the contributions both from

Table 2
Our Frequency-Dependent Model Validation on Samples and Its Model-Fitted Parameters

Sample ID in Figure 4	Sample ID in literature	Consolidation type	Salinity (S/m or M)	σ_c^∞ (S/m)	σ_c^0 (S/m)	τ_c (s)	c_c (−)	A (μF)	K (−)
4a and 4b	PS1	Rock	0.105	0.0082	0.0062	0.0012	0.49	1.57	0.55
4a and 4b	PS1	Rock	0.235	0.0093	0.0072	0.0014	0.52	1.04	0.63
4a and 4b	PS1	Rock	0.494	0.0115	0.0091	0.0016	0.59	1.23	0.63
4c and 4d	MtG	Soil	0.00139	0.5647	0.5544	0.0106	0.51	402.6	0.33
4c and 4d	MtG	Soil	0.0153	0.5137	0.5032	0.0114	0.57	504.1	0.33
4c and 4d	MtG	Soil	0.146	0.4791	0.4646	0.0130	0.54	295.4	0.42

Note. Salinities of PS1 are expressed by S/m, while salinities for MtG are in M. These two samples are exactly the same sample as in Table 1 where their effective medium model parameters can be found.

pore water and EDL, which restricts its usage in quantitative estimations. Given the fact the Cole-Cole is a micro-scale model for σ_c^*, we combine Equation 9 and the micro-scale Equation 11 to derive the salinity- and frequency-dependent model as

$$\sigma^* = \frac{\sigma_w}{F} + \frac{(2\xi_w + 1)\sigma_c^* \sigma_w + 2(1 - \xi_w)\sigma_c^{*2}}{(2 + \xi_w)\sigma_c^* + (1 - \xi_w)\sigma_w}, \quad \sigma_c^* = \sigma_c^\infty + \frac{\sigma_c^0 - \sigma_c^\infty}{1 + (i\omega\tau_c)^{c_c}}, \tag{12}$$

where the parameters $\sigma_c^*, \sigma_c^0, \sigma_c^\infty, \tau_c$, and c_c signify literally the same properties as in Equation 11 but now for EDLs rather than the whole rock/soil, and, as from Soininen (1984), although $\sigma_c^0 \neq \sigma^0$ and $\sigma_c^\infty \neq \sigma^\infty$, mostly $\tau_c \approx \tau$ and $c_c \approx c$.

Figures 4a–4d exhibit the non-linear frequency-dependent SIP responses of a clayey rock and a clayey soil sample that are exactly the same samples employed in the preceding salinity-dependent model validations, that is, the Portland sandstone PS1 from Niu, Revil, and Saidian (2016) and the green montmorillonite MtG from Mendieta et al. (2021), respectively. Before conducting any model tests, as readily seen in Figure 4, the anomalous quadrature responses that surge up at 100 Hz and dominate above 1,000 Hz must be dealt with. Although some may attribute this to Maxwell-Wagner polarization and use an additional high-frequency permittivity $i\omega\varepsilon_\infty$ or another high-frequency Cole-Cole model to describe this, it has been rigorously proved that this anomaly results chiefly from E&EM coupling (Breede et al., 2012; Zimmermann et al., 2008), more specifically, mainly from the coupling between the heterogenous contact impedance of electrodes and the input capacitance of the instrument (Huisman et al., 2016; Wang & Slater, 2019; Zimmermann & Huisman, 2024). That is, above 100 Hz, the response contains two contributions: (a) Inevitable E&EM coupling noises, no matter non-polarizable or retracted electrodes are used; (b) Maxwell-Wagner polarization, mostly the former being comparable with or larger than the latter unless some sophisticated coupling removal tactics are conducted (Huisman et al., 2016; Wang & Slater, 2019). This statement also gets support from the various model investigation of Kruschwitz et al. (2010) where they find that just one Cole-Cole model with the term $i\omega\varepsilon_\infty$ cannot explain the data, while two Cole-Cole models are not recommended because of insufficient parameter sensitivity (i.e., for lack of another peak at high frequencies). In contrast, Kruschwitz et al. (2010) introduces a combination of the asymmetric Cole-Davidson model (Davidson & Cole, 1951; Pelton et al., 1983) and the term $i\omega\varepsilon_\infty$ to provide a good fit to all the data therein, albeit they restate that this model lacks theoretical basis and is essentially a phenomenological one.

It appears that there is neither well-grounded approaches to exclude nor well-established models to include such a high-frequency anomaly in the IP community. Here we resort to the community of colloid science, where Fricke (1932) and Fricke and Curtis (1937) discover that a wedge term of $A(i\omega)^k$ (i.e., the Kth power rule) can satisfactorily explain both the contact coupling effects and the Maxwell-Wagner polarization of many colloids and suspensions such as starch, cellulose, and kaolin, following which Hanai (1968) confirms that bentonite also follows this wedge-type behavior at these frequencies and its total multi-frequency response can be readily explained via overlapping such a wedge-type term with a Cole-Cole model. Given those theoretical basis and experimental evidence from that community, here we add this wedge-type term to our model Equation 12 to exclude both the E&EM coupling and the Maxwell-Wagner polarization. As the model-fitted curves and

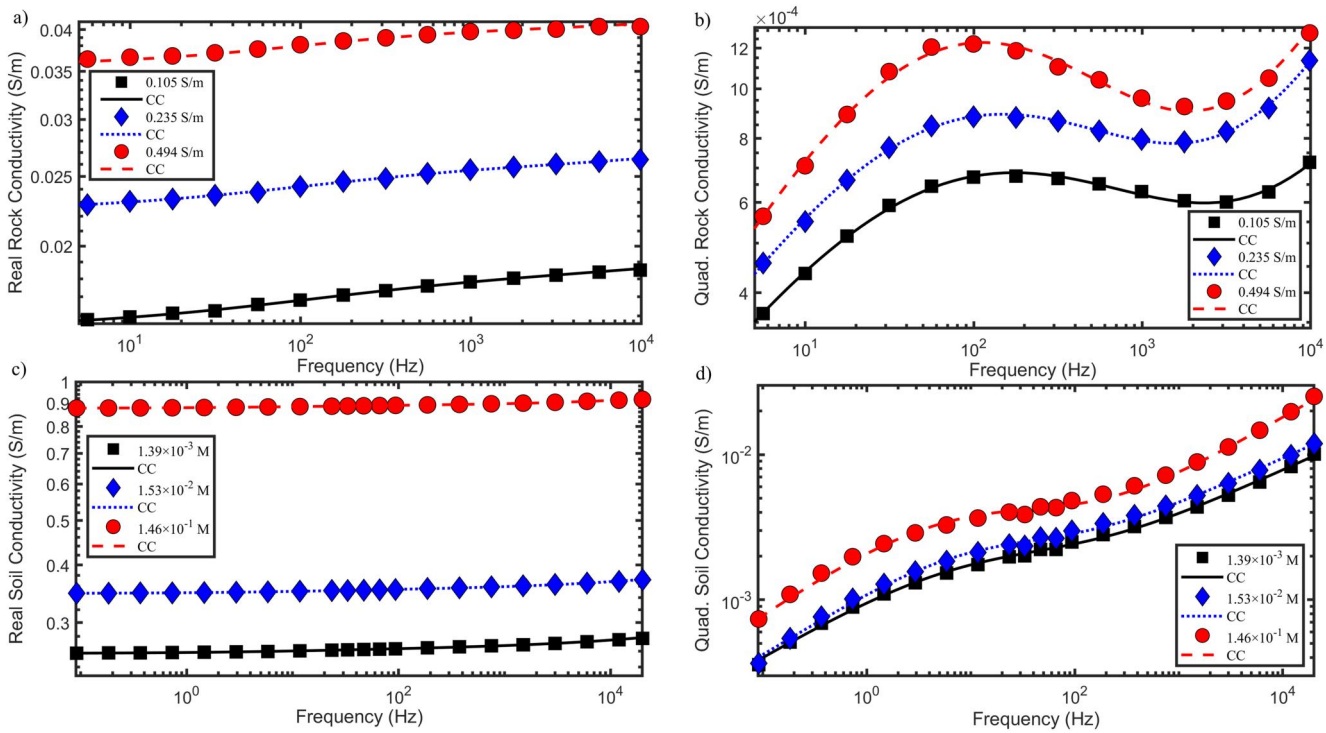

Figure 5. Conventional Cole-Cole model test on the same rock and soil data as in Figure 4, panels (a, b) and (c, d) being the complex conductivities of the Portland sandstone PS1 of Niu, Revil, and Saidian (2016) and the green montmorillonite MtG of Mendieta et al. (2021), respectively. Note that the only difference between here and Figure 4 is that the empirical macro-scale Cole-Cole model is used herein.

parameters are respectively demonstrated in Figure 4 and Table 2, our model works on these measurements very well with coefficient $R^2 > 0.99$.

To demonstrate the physical difference between the empirical macro-scale Cole-Cole model and our model (i.e., the developed effective medium model with theoretical micro-scale Cole-Cole model), the wedge term $A(i\omega)^k$ is also added to the conventional Cole-Cole model of Equation 11 and tested on these measurements with their curves and parameters shown in Figure 5 and Table 3, respectively. As expected, Figures 4 and 5 are almost twins with an indiscernible difference since both models can explain these measurements in mathematics, but, by contrast, they yield these results with different parameters in physics. As clearly compared in Tables 2 and 3, $\sigma_c^0 \neq \sigma^0$ and $\sigma_c^\infty \neq \sigma^\infty$, but $\tau_c \approx \tau$ and $c_c \approx c$, which is completely in accordance with the theory of Soininen (1984). As stressed in the preceding theoretical analysis, Cole-Cole model is essentially a micro-scale model for EDLs, thus, if Cole-Cole model is empirically applied to macro-scale rock/soil, its parameter σ^∞ and σ^0 will be contributed by both the bulk and EDLs and consequently differ from the effective EDL conductivity σ_c^∞ and σ_c^0, while $\tau_c \approx \tau$ and $c_c \approx c$ are just a physical blessing because pore water itself is almost non-polarizable at those low

Table 3
Empirical Macro-Scale Cole-Cole Model Test on Samples and Its Model-Fitted Parameters

Sample ID in Figure 5	Sample ID in literature	Consolidation type	Salinity (S/m or M)	σ^∞ (S/m)	σ^0 (S/m)	τ (s)	c (−)	A (μF)	K (−)
5a and 5b	PS1	Rock	0.105	0.0185	0.0153	0.0013	0.49	1.54	0.55
5a and 5b	PS1	Rock	0.235	0.0261	0.0223	0.0015	0.52	1.10	0.62
5a and 5b	PS1	Rock	0.494	0.0402	0.0356	0.0017	0.59	1.26	0.63
5c and 5d	MtG	Soil	0.00139	0.2614	0.2568	0.0106	0.51	402.6	0.33
5c and 5d	MtG	Soil	0.0153	0.3515	0.3468	0.0115	0.58	513.7	0.33
5c and 5d	MtG	Soil	0.146	0.8889	0.8766	0.0129	0.54	288.9	0.42

Note. Salinities of Sample PS1 are expressed by S/m, while salinities of MtG are in M.

frequencies (Luo & Zhang, 1998). To dissect the SIP responses of composite clayey rocks/soils with the aim of acquiring the intrinsic EDL properties, a theoretical-based effective medium model must be utilized and this is indeed how our presented model works.

More corroboration can be found if the two samples' model-fitted parameters are compared with their source literature. Niu, Revil, and Saidian (2016) employs another theoretical-based model of BHS to model-fit these clayey rock data and obtain $\sigma_c = 0.0113$ S/m during their multi-salinity analysis and confirms that this σ_c value is consistent with their improved SLP model for EDLs, which is not only comparable with our $\sigma_c = 0.0095$ S/m in our previous multi-salinity analysis, but also commensurate with our σ_c^∞ and σ_c^0 here at three different salinities in Table 3. The increase of σ_c^∞ and σ_c^0 with salinities also coincides with their SLP theory that salinity does increase the effective EDL conductivity, albeit this is not the dominant cause of the salinity-dependent nonlinearity of clayey rocks/soils (Niu, Revil, & Saidian, 2016). As to the characteristic relaxation time τ, Warburg decomposition assisted by polynomials are used therein to capture these relaxation times at different salinities, whose values are in line with ours in Table 3 as well. Both ours and their relaxation times manifest a weak but visible increase under these intermediate salinities (e.g., between 0.05 S/m and 1 S/m). Given the generally accepted relationship of $\tau = \Lambda^2/2D$, where Λ is the characteristic pore/grain radius and D is the diffusion coefficient for ions in the EDL, and the fact that no appreciable forces change Λ under these intermediate salinities, such an increase of relaxation time with salinities should result from the change of diffusion coefficient D with salinities, such as the shrinkage of diffuse layer and its influences to Stern layer, that is, the integrated influences of DLP and SLP (Lyklema et al., 1983; Niu, Revil, & Saidian, 2016).

As to the clayey soil data analysis by Mendieta et al. (2021), we find that our σ^0 values from conventional Cole-Cole model (Table 3 herein) are exactly the same as their σ^0 values (Table 4 therein), but these relaxation time τ values are different. This is reasonable because double-Pelton model (the same as double-Cole-Cole model if works on complex resistivity rather than complex conductivity data, cf., Macnae, 2015) is employed therein. As discussed by Kruschwitz et al. (2010), double-Cole-Cole model is not suggested because there is not enough information to model-fit the high-frequency Cole-Cole one for lack of another peak in mathematics. In reality, from the colloid science community (Fricke & Curtis, 1937; Hanai, 1968), such a high-frequency peak doesn't exist but behaves as a wedge shape in physics. That means, with the double-Cole-Cole model, the high-frequency Cole-Cole model will influence the low-frequency Cole-Cole model-fitting in an unpredictable way. Considering the information of σ^0 is mainly at the lowest frequencies so that its influence is negligible, we get the same σ^0 values as theirs. However, the relaxation time τ is rather sensitive to this influence such that the indeterminate high-frequency Cole-Cole model drags the low-frequency peak into a higher frequency, which makes their relaxation time τ smaller than ours. Nonetheless, both ours and theirs reveal a weak but non-neglectable increase of relaxation times with growing salinities, which is in accord with the above analysis of the sandstone sample PS1. Another apparent feature of our σ_c^∞ and σ_c^0 is that, different to the clayey rock PS1, they obviously decrease with salinities. This phenomenon is rather rational if we keep in mind that this clayey soil sample MtG is green montmorillonite with a high purity of 90%. For such pure clays, as evidenced in Palomino and Santamarina (2005) and also Mendieta et al. (2021), clay aggregation actively occurs with the increase of salinities (e.g., edge-to-face aggregation at intermediate salinities), which inevitably decreases the effective EDL conductivities σ_c^∞ and σ_c^0. Indeed, this strongly exhibits the advantage of our model because, as from Tables 2 and 3, empirically using macro-scale Cole-Cole model always obtain an increase of σ^∞ and σ^0 with increasing salinities no matter how EDLs change, as the bulk water conductivity σ_w dominates this term, but, by contrast, our model has the ability to extract decreasing effective EDL conductivities σ_c^∞ and σ_c^0 from increasing salinities, as our developed effective medium model completely separates EDLs from the bulk water.

Although in our aforementioned analysis, micro-scale Cole-Cole model is employed for EDLs. In much the same vein, we can fuse micro-scale Debye/Warburg decomposition into Equations 9/10, which would be advantageous when grain/pore sizes don't distribute in a log-normal way that Cole-Cole model presumes (Cole & Cole, 1941). Note that, granted, Equations 9–12 are novel for their first appearance, but such a micro-to-macro upscaling philosophy by means of an effective medium model exists elsewhere, for example, Leroy et al. (2017), Lesmes and Morgan (2001), and Niu, Revil, and Saidian (2016) integrate Debye/Warburg decomposition into the BHS model (Sen et al., 1981) to implement this upscaling. BHS model is a well-established effective medium model that has its roots in the differential effective medium (DEM) theory. That being said, as it turns out in the following section, BHS bears several disadvantages as an effective medium model for IP.

3. Comparisons With Other Models

Comparisons with 12 existing models, including BHS and three-resistor models, exhibit the mathematical and physical advantages of Equation 9 in the real domain (Qi & Wu, 2022). Here we proceed to corroborate that such advantages still hold in the complex domain.

3.1. Weller-Slater and Three-Resistor Models

Weller and Slater (2012) generalize from the SLP model of Skold et al. (2011) to develop the quadrature conductivity model as

$$\sigma'' = c_s + \left(a_s \frac{\sigma_w}{b_s + \sigma_w}\right), \tag{13}$$

where a_s, b_s, and c_s are fitting parameters, which explain measurements excellently. Although Skold et al. (2011) declare c_s (proton hopping process) is important merely at low pH and only a_s relates to S_{por}, it is found that c_s is mandatory in model-fitting (Weller & Slater, 2012) and, surprisingly, a_s, b_s, and c_s all linearly relates to S_{por} (Weller, Zhang, & Slater, 2015). Such a paradox can be perfectly explained via the comparison with the second term of Equation 9 as

$$a_s = \frac{9\xi_w}{(2+\xi_w)(1-\xi_w)}\sigma_c^*,\ b_s = \frac{2+\xi_w}{1-\xi_w}\sigma_c^*,\ \text{and}\ \ c_s = \frac{2(1-\xi_w)}{2+\xi_w}\sigma_c^*, \tag{14}$$

where all three parameters are functions of σ_c^* and thus S_{por}. Considering the striking evidence that the SLP model of Skold et al. (2011) cannot explain its generalized Well-Slater model but our model explains it so well, it is legitimate to deduce that the non-linear increase in quadrature conductivity is caused by the composite geometry (i.e., effective medium models) rather than the EDL variation, as it is almost impossible that all these things happen by accident.

Furthermore, if we recall the three-resistor model for the real conductivity (Lévy et al., 2018; Wyllie & Southwick, 1954)

$$\sigma' = \frac{\sigma_w}{F} + \frac{(y+z)\sigma_c\sigma_w + x\sigma_c^2}{xz\sigma_c + yz\sigma_w}, \tag{15}$$

where x, y, and z are empirical factors. It can be easily tested that the second term of three-resistor model equals Weller-Salter model, which are the real (Qi & Wu, 2022) and quadrature parts of Equation 9, respectively. It is not surprising that three-resistor and Weller-Slater models work so well for SIP since our model reconciles these two models with the fact that surface and quadrature conductivities follow the same EDL-and-water pattern as in Equation 9, such similarity being phenomenologically discovered by Börner (1992) and confirmed by Weller et al. (2013) and Lévy et al. (2019).

3.2. Waxman-Smits and Vinegar-Waxman Models

Through massive experiments, Waxman and Smits (1968) empirically develop an electrical conductivity model and Vinegar and Waxman (1984) extend it into IP as

$$\sigma^* = \frac{\sigma_w}{F} + \frac{BQ_v}{F} + i\frac{\lambda Q_v}{F\phi}, \tag{16}$$

where $F\phi$ is the so-called electrical tortuosity. To make it non-linear, they postulate that B and λ increase exponentially with salinity, which conflicts with electrochemistry (Johnson & Sen, 1988). Although some (Johnson et al., 1986; Revil, 2013) attempt to theoretically re-derive Equation 16, coupling between EDL and water is neglected, which opposes Maxwell's equations. Surprisingly, despite these drawbacks, Equation 16 dominates the community as the most popular model.

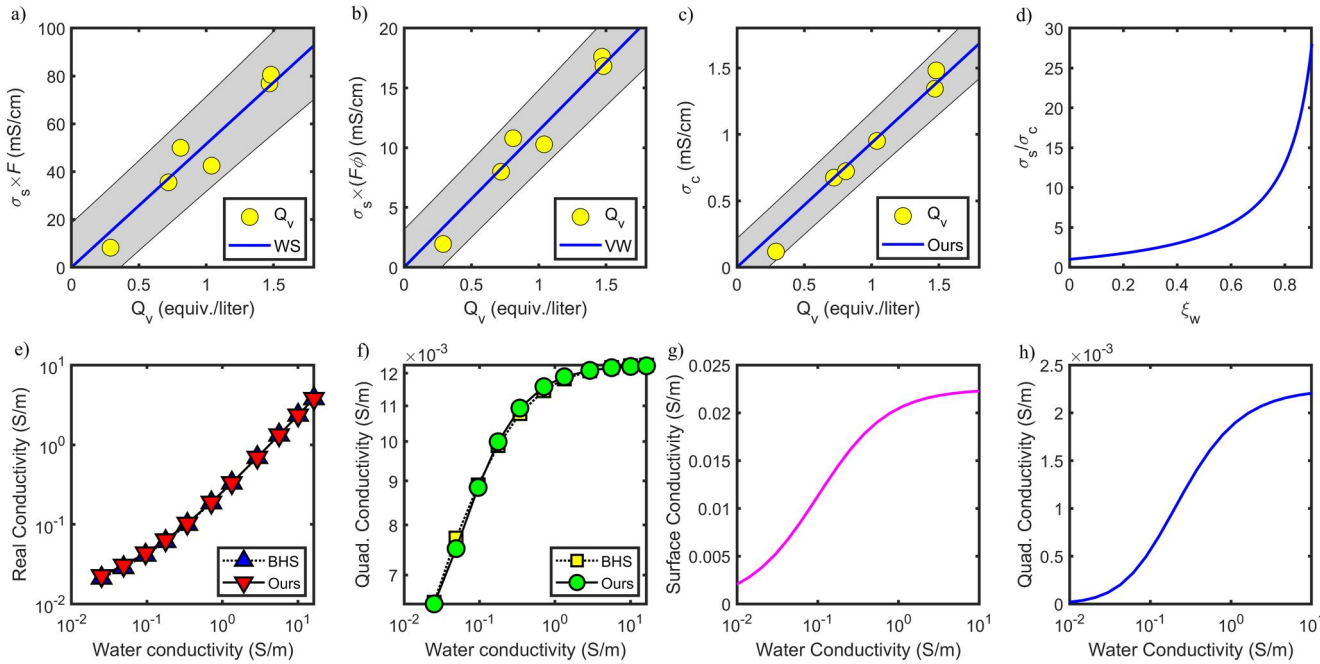

Figure 6. Comparisons with other models. Panels (a–c) are parametric correlations of Waxman-Smits ($R^2 = 0.93$), Vinegar-Waxman ($R^2 = 0.95$), and ours ($R^2 = 0.97$) on the Lower Tertiary shaly samples from Waxman and Smits (1968), where shaded bands represent the 95% confidence intervals. Panel (d) is the variation of our high-salinity coefficient σ_s/σ_c. Panels (e and f) manifest the consistency between BHS ($\phi = 0.4$, $m = 1.6$, and $\sigma_c = 0.018 + 0.01i$ S/m) and ours ($F = 4.3$, $\xi_w = 18\%$, and $\sigma_c = 0.015 + 0.0074i$ S/m), while (g) and (h) shows surface and quadrature conductivities of diluted suspensions with a constant EDL ($p = 0.05$, $F = 1 + 1.5p = 1.075$, $\Lambda = 10^{-8}$ m, and $\Sigma_s^* = 10^{-9} + 10^{-10}i$ S), respectively.

True formation factor F is a parameter characterizing the pore-water topology and, for clayey rocks/soils, F is notionally the value if clays were replaced by a geometrically identical but insulating matrix (Worthington, 1985), which makes it hard to credit that F or $F\phi$ is entangled in σ_s. To show how Equation 16 disguises the fact, experiments from Waxman and Smits (1968) are employed to compare Equations 9 and 16 in Figures 6a–6c. Although our model performs the best with the largest R^2, apparently all manifest linear features with Q_v. However, "Correlation does not imply causation." Such correlation cannot confirm adding F or $F\phi$ is physically tenable since σ_s itself already holds a pseudo-linear correlation with Q_v. As a matter of fact, when these data of Waxman and Smits (1968) are model-fitted with the well-established BHS model, its causal relationship ratio of $\sigma_c - Q_v$ is around 0.9 (cf., Figure 8 in Bussian, 1983; Figure 5 in de Lima & Sharma, 1990), which coincides pretty well with our model (Figure 6c) but differs vastly from Waxman models (Figures 6a and 6b). Thus, although adding F or $F\phi$ in σ_s may make such a pseudo-linear correlation seemingly coherent, this is just a mathematical coincidence that leads to this phenomenon, as at high-salinity, our model becomes

$$\sigma^* = \frac{\sigma_w}{F} + \frac{2\xi_w + 1}{1 - \xi_w}\sigma_c^*, \tag{17}$$

where $(2\xi_w + 1)/(1 - \xi_w)$ falls into the same order of magnitude as F or $F\phi$ (Figure 6d).

3.3. Bruggeman-Hanai-Sen (BHS) Model and Dukhin Number

BHS model (Bruggeman, 1935; Hanai, 1960; Sen et al., 1981)

$$\sigma^* = \sigma_w \phi^m \left(\frac{1 - \sigma_c^*/\sigma_w}{1 - \sigma_c^*/\sigma^*}\right)^m \tag{18}$$

is an exceptional precedent that can both explain real and quadrature nonlinearities concurrently, and it downscales to Archie's law when in the one-phase situation. Compared to such an eminent model, as discussed in Qi

and Wu (2022), Equation 9 bears the advantages of mathematical simplicity and parametric consistency with Archie's law. The former is because BHS is an implicit function with σ^* on both sides that needs complicated methods to solve (Glover et al., 2010; Lesmes & Morgan, 2001), while the latter results from its parameter m links to both bulk and surface continuity (de Lima et al., 2005; Niwas et al., 2006, 2007). It is deduced that these disadvantages make BHS not as popular as Waxman-type models. Nonetheless, the physical basis of BHS is similar to ours that both attributes such salinity-dependent nonlinearity to the composite geometry. To confirm such consistency, simulated SIP curves of BHS and ours are comparably shown in Figures 6e and 6f where both models corroborate constant EDL can cause such nonlinearity via the similar parameter σ_c^*, which is in accord with the above-mentioned fact that these two models obtain similar causal ratios of $\sigma_c - Q_v$ from the same data of Waxman and Smits (1968).

To provide more evidence, it is worth quoting Stanislav Dukhin, the introducer of Dukhin number Du, a dimensionless number quantifying the relative importance of surface conduction (Lyklema, 1995, 2002). Although some write Du as σ_s/σ_w, this contradicts Dukhin's own definition

$$Du = \frac{\Sigma_s}{\Lambda \sigma_w}. \tag{19}$$

In the landmark work of Dukhin and Derjaguin (1974), obviously they sensed σ_s is a mixed parameter involving both EDL and water. To refute Waxman-type models, they even derived analytic expressions for several examples such as dilute spherical suspensions

$$\sigma = \frac{\sigma_w}{F} + \frac{9\sigma_w}{2} p \frac{Du}{1 + Du}, \tag{20}$$

where p is the volume fraction of suspended spheres, which clearly evidences that F or $F\phi$ doesn't participate in σ_s and constant EDL can generate such non-linear increases for both surface and quadrature conductivities (Figures 6g and 6h). Unfortunately, this seemed to receive little attention from the IP community.

4. Discussions and Conclusions

Here we discuss and conclude with three points as follows.

4.1. Definition of Complex Surface Conductivity

Complex surface conductivity σ_s^*, real part normally being called surface conductivity σ_s and imaginary part being quadrature conductivity σ'', is the remaining complex conductivity when subtracting the bulk water conductivity (i.e., Archie's law σ_w/F) from the bulk complex conductivity of clayey rocks/soils σ^*. The discovery of this remaining term can be traced back to Patnode and Wyllie (1950), and it has been generally accepted that such a remaining complex conductivity σ_s^* is caused by the EDL at the interface between the solid phase and fluid since the first-ever EDL ascription by Winsauer and McCardell (1953). However, the fact that EDL is the source of σ_s^* by no means implies that σ_s^* would be an exclusive parameter merely linked to EDL property because, as evidenced in the preceding sections, the existence of EDL disturbs the normal field in water and thus, the most important, it is essentially the total field in water that is measured for IP, which consists of the normal field (i.e., bulk water conductivity being expressed by Archie's law) and the abnormal field (i.e., complex surface conductivity being expressed by Maxwell Garnett equation). Given that σ_s^* is a composite parameter under the interplay of EDL and water is dictated by the underlying principle of Maxwell's equations and is validated through theories, simulations, experiments, and comparisons (i.e., the four ways to substantiate a new model in science), which shall be solid and convincing.

Previous complex conductivity models for clayey rocks and soils mostly either exclusively ascribe σ_s^* to the sole EDL (e.g., Waxman-type models) or empirically express σ_s^* with redundancy parameters (e.g., three-resistor model), among which, BHS model stands out as an excellent model with roots in the DEM theory and works pretty well in practice. In fact, both BHS and ours ascribe the salinity-dependent nonlinearity mainly to the geometry and both employ the Maxwell Garnett equation in their effective medium model development yet in slightly different ways. Sen et al. (1981) use Maxwell Garnett equation (i.e., Equation 12 therein) as the basic

equation to describe a grain coated with a water shell (water being the host and solid being the guest) and then infinitely add such a grain-with-shell in a differential form (i.e., DEM) to finally develop the exceptional BHS model, while we choose another avenue of first subtracting the bulk water conduction (i.e., Archie's law) and then only adopting Maxwell Garnett equation (solid being the host and water being the guest, as previously discussed) to adequately express the remaining complex surface conductivity σ_s^*, with which we separate the bulk and surface properties explicitly in physics and make our model simple in mathematics. By and large, our model supports the well-established BHS model and provides a viable alternative for such a prominent model.

4.2. Importance of the Nonlinearity

Although rather simple non-linear models are presented, such nonlinearity is more important than it seems. As is known, one main reason for conducting IP rather than E&EM methods is the aspiration to separate bulk and interface properties, such as to assess the porosity and permeability, the former being assessed through the formation factor F and the latter being estimated via S_{por} or Λ within σ_c^*. Unfortunately, as evidenced in Equations 9/10, F and σ_c^* cannot be accurately model-fitted without the non-linear portion. One may argue that, since the non-linear model approximates the linear model of Equation 17 at relatively high salinity, simpler linear model with linear-portion data works as well. Unfortunately, two problems immediately emerge from such a treatment: (a) The transition from non-linear portion to linear portion is difficult to discern such that including any data in the non-linear portion during a linear model-fitting will lead to an apparent formation factor F' that is always smaller than the true formation factor F (Qi & Wu, 2022); (b) It is impossible to extract the parameter ξ_w by a linear model-fitting with the linear-portion data because the information of ξ_w is intrinsically contained in the non-linear portion.

Fortunately, the attention to such nonlinearity doesn't increase the workload considerably, as even for the conventional linear model-fitting, multi-salinity measurements are still mandatory to get the formation factor F, otherwise F has to be estimated empirically. Taking the nonlinearity into consideration doesn't change anything of the routine multi-salinity measurement except that the salinities shall include some relatively lower ones such that the non-linear portion can be acquired, one caveat being that those salinities shall be chosen neither too low nor too high, as at extremely low salinity (e.g., <0.05 S/m) EDL varies violently and at exceedingly high salinity (e.g., >1 S/m) a strong decrease of σ_s^* occurs.

4.3. Application of Our Models

EDL almost exists at the interface between any material and interstitial fluid, even for silica (Hao et al., 2015; Peruzzo et al., 2018). Although our non-linear models are presented for clayey rocks and soils, it stands to reason that they also apply to other ionically conductive materials in the IP realm as long as the EDL and geometry change negligibly. For example, carbonates are another group of rocks and soils that are being extensively investigated by IP practitioners for karst aquifers of groundwater (Bücker et al., 2021; Šumi, 1965), carbonate reservoirs of oil (Deng et al., 2022; Schmutz et al., 2012), enhanced calcite precipitation (Saneiyan et al., 2021; Wu et al., 2011), and carbon dioxide sequestration (Börner et al., 2017; Kremer et al., 2016), to name but a few. Likewise, salinity-dependent nonlinearity has also been observed for carbonates (Panwar et al., 2021; Saner & Akbar, 2010). Given the fact that such nonlinearity is a natural consequence of the EDL-and-water coupling, this nonlinearity of carbonates should also result mainly from the geometry (effective medium model), albeit EDL varies to some degree.

Besides rocks and soils, biological application is an emerging area in the IP community (Atekwana & Slater, 2009; Ehosioke et al., 2020; Loiseau et al., 2023; Peruzzo et al., 2021; Song et al., 2022; Zhang et al., 2014). Although we believe that for those micro-organisms and plant roots, the EDL-and-water pattern still holds on condition that there are no electronically conductive materials (e.g., pyrite, metals, and some carbon allotropes), our model application becomes more complicated in this scenario, as multi-salinity experiments are impractical to realize for living organisms. One may argue that multi-frequency measurement is sufficient in its own right, but as illustrated in the previous sections, without the employment of an effective medium model, purely fitting multi-frequency data alone output parameters that mingle bulk and interface together, as Cole-Cole and Debye/Warburg decomposition models are indeed the genuine relaxation models for micro-scale EDLs rather than macro-scale materials. To substitute for the multi-salinity measurement, some empirical or semi-empirical

approaches, such as computer simulations (Bücker et al., 2019; Niu, 2023; Tsukanov & Schwartz, 2021), may be practical alternatives.

In conclusion, from basic principles, we prove that surface and quadrature conductivities of clayey rocks and soils are composite properties under the interplay of EDL and water, to separate which, we develop salinity- and frequency-dependent non-linear models that are substantiated through theories, experiments, simulations, and comparisons. Given that such nonlinearity is an inevitable corollary of Maxwell's equations, our non-linear models may also apply to other EDL-bearing electrolytic materials, providing that EDL variation and geometry change are negligibly small. We expect our models could improve the comprehension of IP mechanisms and shape the future quantitative IP applications.

Data Availability Statement

Data used in this study can be found in the previously published literature of Börner (1992), Niu, Revil, and Saidian (2016), Slater and Glaser (2003), Mendieta et al. (2021), and Waxman and Smits (1968). Materials for the models and results presented in this paper are available in Qi and Wu (2023).

Acknowledgments
Funding for this research is provided by the U.S. Department of Energy, Office of Science, Office of Basic Energy Sciences, Chemical Sciences, Geosciences, and Biosciences Division, through its Geoscience program at LBNL under contract DE-AC02-05CH11231. The authors thank the three Editors (JGR Editor Dr. Douglas Schmitt, JGR Associate Editor, and GRL Editor Dr. Daoyuan Sun) and the three reviewers (Two anonymous and Dr. Andreas Weller) for their valuable comments and discussions.

References

Archie, G. E. (1942). The electrical resistivity log as an aid in determining some reservoir characteristics. *Transactions of the AIME*, *146*(01), 54–62. https://doi.org/10.2118/942054-G

Atekwana, E. A., & Slater, L. D. (2009). Biogeophysics: A new Frontier in Earth science research. *Reviews of Geophysics*, *47*(4), RG4004. https://doi.org/10.1029/2009RG000285

Bernabé, Y., & Revil, A. (1995). Pore-scale heterogeneity, energy dissipation and the transport properties of rocks. *Geophysical Research Letters*, *22*(12), 1529–1532. https://doi.org/10.1029/95GL01418

Binley, A., Hubbard, S. S., Huisman, J. A., Revil, A., Robinson, D. A., Singha, K., & Slater, L. D. (2015). The emergence of hydrogeophysics for improved understanding of subsurface processes over multiple scales. *Water Resources Research*, *51*(6), 3837–3866. https://doi.org/10.1002/2015WR017016

Binley, A., & Slater, L. (2020). *Resistivity and induced polarization: Theory and applications to the near-surface Earth*. Cambridge University Press.

Börner, F. D. (1992). *Complex conductivity measurements of reservoir properties*. Advances in Core Evaluation III (Reservoir Management). Gordon and Breach Science Publishers. Retrieved from http://www.jgmaas.com/SCA/1992/1-SCA1992-18EURO.pdf

Börner, F. D., Schopper, J. R., & Weller, A. (1996). Evaluation of transport and storage properties in the soil and groundwater zone from induced polarization measurements. *Geophysical Prospecting*, *44*(4), 583–601. https://doi.org/10.1111/j.1365-2478.1996.tb00167.x

Börner, J. H., Herdegen, V., Repke, J. U., & Spitzer, K. (2017). Spectral induced polarization of the three-phase system CO_2-brine-sand under reservoir conditions. *Geophysical Journal International*, *208*(1), 289–305. https://doi.org/10.1093/gji/ggw389

Breede, K., Kemna, A., Esser, O., Zimmermann, E., Vereecken, H., & Huisman, J. A. (2012). Spectral induced polarization measurements on variably saturated sand-clay mixtures. *Near Surface Geophysics*, *10*(6), 479–489. https://doi.org/10.3997/1873-0604.2012048

Brown, W. F., Jr. (1955). Solid mixture permittivities. *The Journal of Chemical Physics*, *23*(8), 1514–1517. https://doi.org/10.1063/1.1742339

Brown, W. F., Jr. (1965). Dielectric constants, permeabilities, and conductivities of random media. *Transactions of the Society of Rheology*, *9*(1), 357–380. https://doi.org/10.1122/1.549016

Bruggeman, D. A. G. (1935). Berechnung verschiedener physikalischer Konstanten von heterogenen Substanzen. I. Dielektrizitätskonstanten und Leitfähigkeiten der Mischkörper aus isotropen Substanzen. *Annalen der Physik*, *416*(7), 636–664. https://doi.org/10.1002/andp.19354160705

Bücker, M., Flores Orozco, A., Gallistl, J., Steiner, M., Aigner, L., Hoppenbrock, J., et al. (2021). Integrated land and water-borne geophysical surveys shed light on the sudden drying of large karst lakes in southern Mexico. *Solid Earth*, *12*(2), 439–461. https://doi.org/10.5194/se-12-439-2021

Bücker, M., Flores Orozco, A., Undorf, S., & Kemna, A. (2019). On the role of Stern-and diffuse-layer polarization mechanisms in porous media. *Journal of Geophysical Research: Solid Earth*, *124*(6), 5656–5677. https://doi.org/10.1029/2019JB017679

Bussian, A. E. (1983). Electrical conductance in a porous medium. *Geophysics*, *48*(9), 1258–1268. https://doi.org/10.1190/1.1441549

Carman, P. C. (1937). Fluid flow through a granular bed. *Transactions of the Institution of Chemical Engineers*, *15*, 150–156. https://doi.org/10.1016/S0263-8762(97)80003-2

Christensen, N. B. (1997). Electromagnetic subsurface imaging. A case for an adaptive Born approximation. *Surveys in Geophysics*, *18*(5), 477–510. https://doi.org/10.1023/A:1006593408478

Cole, K. S., & Cole, R. H. (1941). Dispersion and absorption in dielectrics I. Alternating current characteristics. *The Journal of Chemical Physics*, *9*(4), 341–351. https://doi.org/10.1063/1.1750906

Cosenza, P., Ghorbani, A., Camerlynck, C., Rejiba, F., Guérin, R., & Tabbagh, A. (2009). Effective medium theories for modelling the relationships between electromagnetic properties and hydrological variables in geomaterials: A review. *Near Surface Geophysics*, *7*(5–6), 563–578. https://doi.org/10.3997/1873-0604.2009009

Davidson, D. W., & Cole, R. H. (1951). Dielectric relaxation in glycerol, propylene glycol, and n-propanol. *The Journal of Chemical Physics*, *19*(12), 1484–1490. https://doi.org/10.1063/1.1748105

de Lima, O. A., Clennell, M. B., Nery, G. G., & Niwas, S. (2005). A volumetric approach for the resistivity response of freshwater shaly sandstones. *Geophysics*, *70*(1), F1–F10. https://doi.org/10.1190/1.1852771

de Lima, O. A., & Sharma, M. M. (1990). A grain conductivity approach to shaly sandstones. *Geophysics*, *55*(10), 1347–1356. https://doi.org/10.1190/1.1442782

Deng, Y., Qian, J., Luo, Q., Ma, H., Ma, L., & Xu, K. (2022). Effects of grain size, solution salinity and pH on the electrical response of oil-bearing carbonate sands. *Near Surface Geophysics*, *20*(3), 253–264. https://doi.org/10.1002/nsg.12201

Dukhin, S. S., & Derjaguin, B. V. (1974). Electrokinetic phenomena. In E. Matijević (Ed.), *Surface and colloid science* (Vol. 7). Wiley.

Dukhin, S. S., Zimmermann, R., & Werner, C. (2012). Surface conductivity. In H. Ohshima (Ed.), *Electrical phenomena at interfaces and biointerfaces: Fundamentals and applications in nano-, bio-, and environmental sciences* (pp. 95–126). Wiley.
Ehosioke, S., Nguyen, F., Rao, S., Kremer, T., Placencia-Gomez, E., Huisman, J. A., et al. (2020). Sensing the electrical properties of roots: A review. *Vadose Zone Journal*, *19*(1), e20082. https://doi.org/10.1002/vzj2.20082
Fiandaca, G., Auken, E., Christiansen, A. V., & Gazoty, A. (2012). Time-domain-induced polarization: Full-decay forward modeling and 1D laterally constrained inversion of Cole-Cole parameters. *Geophysics*, *77*(3), E213–E225. https://doi.org/10.1190/geo2011-0217.1
Fricke, H. (1932). XXXIII. The theory of electrolytic polarization. *The London, Edinburgh and Dublin Philosophical Magazine and Journal of Science*, *14*(90), 310–318. https://doi.org/10.1080/14786443209462064
Fricke, H., & Curtis, H. J. (1937). The dielectric properties of water–dielectric interphases. *Journal of Physical Chemistry*, *41*(5), 729–745. https://doi.org/10.1021/j150383a011
Garnett, J. C. M. (1904). XII. Colours in metal glasses and in metallic films. *Philosophical Transactions of the Royal Society of London—A*, *203*, 385–420. https://doi.org/10.1098/rsta.1904.0024
Glover, P. W. J. (2015). Geophysical properties of the near surface Earth: Electrical properties. In G. Schubert (Ed.). *Treatise on geophysics: Resources in the near-surface Earth* (2nd ed., Vol. 11, pp. 89–137). Elsevier.
Glover, P. W. J., Ransford, T. J., & Auger, G. (2010). A simple method for solving the Bussian equation for electrical conduction in rocks. *Solid Earth*, *1*(1), 85–91. https://doi.org/10.5194/se-1-85-2010
Habashy, T. M., Groom, R. W., & Spies, B. R. (1993). Beyond the Born and Rytov approximations: A nonlinear approach to electromagnetic scattering. *Journal of Geophysical Research*, *98*(B2), 1759–1775. https://doi.org/10.1029/92JB02324
Hanai, T. (1960). Theory of the dielectric dispersion due to the interfacial polarization and its application to emulsions. *Kolloid Zeitschrift*, *171*(1), 23–31. https://doi.org/10.1007/BF01520320
Hanai, T. (1968). Electrical properties of emulsions. In P. Sherman (Ed.), *Emulsions science* (pp. 354–477). Academic Press.
Hao, N., Moysey, S. M., Powell, B. A., & Ntarlagiannis, D. (2015). Evaluation of surface sorption processes using spectral induced polarization and a ^{22}Na tracer. *Environmental Science & Technology*, *49*(16), 9866–9873. https://doi.org/10.1021/acs.est.5b01327
Hördt, A., Bairlein, K., Bielefeld, A., Bücker, M., Kuhn, E., Nordsiek, S., & Stebner, H. (2016). The dependence of induced polarization on fluid salinity and pH, studied with an extended model of membrane polarization. *Journal of Applied Geophysics*, *135*, 408–417. https://doi.org/10.1016/j.jappgeo.2016.02.007
Huisman, J. A., Zimmermann, E., Esser, O., Haegel, F. H., Treichel, A., & Vereecken, H. (2016). Evaluation of a novel correction procedure to remove electrode impedance effects from broadband SIP measurements. *Journal of Applied Geophysics*, *135*, 466–473. https://doi.org/10.1016/j.jappgeo.2015.11.008
Johnson, D. L., Koplik, J., & Schwartz, L. M. (1986). New pore-size parameter characterizing transport in porous media. *Physical Review Letters*, *57*(20), 2564–2567. https://doi.org/10.1103/PhysRevLett.57.2564
Johnson, D. L., & Sen, P. N. (1988). Dependence of the conductivity of a porous medium on electrolyte conductivity. *Physical Review B*, *37*(7), 3502–3510. https://doi.org/10.1103/PhysRevB.37.3502
Jougnot, D., Ghorbani, A., Revil, A., Leroy, P., & Cosenza, P. (2010). Spectral induced polarization of partially saturated clay-rocks: A mechanistic approach. *Geophysical Journal International*, *180*(1), 210–224. https://doi.org/10.1111/j.1365-246X.2009.04426.x
Jougnot, D., Revil, A., & Leroy, P. (2009). Diffusion of ionic tracers in the Callovo-Oxfordian clay-rock using the Donnan equilibrium model and the formation factor. *Geochimica et Cosmochimica Acta*, *73*(10), 2712–2726. https://doi.org/10.1016/j.gca.2009.01.035
Kemna, A., Binley, A., Cassiani, G., Niederleithinger, E., Revil, A., Slater, L., et al. (2012). An overview of the spectral induced polarization method for near-surface applications. *Near Surface Geophysics*, *10*(6), 453–468. https://doi.org/10.3997/1873-0604.2012027
Kessouri, P., Furman, A., Huisman, J. A., Martin, T., Mellage, A., Ntarlagiannis, D., et al. (2019). Induced polarization applied to biogeophysics: Recent advances and future prospects. *Near Surface Geophysics*, *17*(6), 595–621. https://doi.org/10.1002/nsg.12072
Kremer, T., Schmutz, M., Maineult, A., & Agrinier, P. (2016). Laboratory monitoring of CO_2 injection in saturated silica and carbonate sands using spectral induced polarization. *Geophysical Journal International*, *207*(2), 1258–1272. https://doi.org/10.1093/gji/ggw333
Kruschwitz, S., Binley, A., Lesmes, D., & Elshenawy, A. (2010). Textural controls on low-frequency electrical spectra of porous media. *Geophysics*, *75*(4), WA113–WA123. https://doi.org/10.1190/1.3479835
Leroy, P., Li, S., Jougnot, D., Revil, A., & Wu, Y. (2017). Modelling the evolution of complex conductivity during calcite precipitation on glass beads. *Geophysical Journal International*, *209*(1), 123–140. https://doi.org/10.1093/gji/ggx001
Leroy, P., & Revil, A. (2009). A mechanistic model for the spectral induced polarization of clay materials. *Journal of Geophysical Research*, *114*(B10), B10202. https://doi.org/10.1029/2008JB006114
Leroy, P., Revil, A., Kemna, A., Cosenza, P., & Ghorbani, A. (2008). Complex conductivity of water-saturated packs of glass beads. *Journal of Colloid and Interface Science*, *321*(1), 103–117. https://doi.org/10.1016/j.jcis.2007.12.031
Lesmes, D. P., & Frye, K. M. (2001). Influence of pore fluid chemistry on the complex conductivity and induced polarization responses of Berea sandstone. *Journal of Geophysical Research*, *106*(B3), 4079–4090. https://doi.org/10.1029/2000JB900392
Lesmes, D. P., & Morgan, F. D. (2001). Dielectric spectroscopy of sedimentary rocks. *Journal of Geophysical Research*, *106*(B7), 13329–13346. https://doi.org/10.1029/2000JB900402
Lévy, L., Gibert, B., Sigmundsson, F., Flóvenz, Ó. G., Hersir, G. P., Briole, P., & Pezard, P. A. (2018). The role of smectites in the electrical conductivity of active hydrothermal systems: Electrical properties of core samples from Krafla volcano, Iceland. *Geophysical Journal International*, *215*(3), 1558–1582. https://doi.org/10.1093/gji/ggy342
Lévy, L., Weller, A., & Gibert, B. (2019). Influence of smectite and salinity on the imaginary and surface conductivity of volcanic rocks. *Near Surface Geophysics*, *17*(6), 653–673. https://doi.org/10.1002/nsg.12069
Loiseau, B., Carrière, S. D., Jougnot, D., Singha, K., Mary, B., Delpierre, N., et al. (2023). The geophysical toolbox applied to forest ecosystems–A review. *Science of the Total Environment*, *899*, 165503. https://doi.org/10.1016/j.scitotenv.2023.165503
Luo, Y., & Zhang, G. (1998). *Theory and application of spectral induced polarization*. Society of Exploration Geophysicists.
Lyklema, J. (1995). *Fundamentals of interface and colloid science, vol II: Solid liquid interfaces*. Academic Press.
Lyklema, J. (2002). The role of surface conduction in the development of electrokinetics. In Á. V. Delgado (Ed.), *Interfacial electrokinetics and electrophoresis* (pp. 87–97). CRC Press.
Lyklema, J., Dukhin, S. S., & Shilov, V. N. (1983). The relaxation of the double layer around colloidal particles and the low-frequency dielectric dispersion: Part I. Theoretical considerations. *Journal of Electroanalytical Chemistry and Interfacial Electrochemistry*, *143*(1–2), 1–21. https://doi.org/10.1016/S0022-0728(83)80251-4
Lyklema, J., Springer, M. M., Shilov, V. N., & Dukhin, S. S. (1986). The relaxation of the double layer around colloidal particles and the low-frequency dielectric dispersion: Part III. Application of theory to experiments. *Journal of Electroanalytical Chemistry and Interfacial Electrochemistry*, *198*(1), 19–26. https://doi.org/10.1016/0022-0728(86)90022-7

Macnae, J. (2015). Comment on: Tarasov, A. & Titov, K., 2013, on the use of the Cole–Cole equations in spectral induced polarization, Geophys. J. Int., 195, 352–356. *Geophysical Journal International*, *202*(1), 529–532. https://doi.org/10.1093/gji/ggv131

Mendieta, A., Jougnot, D., Leroy, P., & Maineult, A. (2021). Spectral induced polarization characterization of non-consolidated clays for varying salinities-An experimental study. *Journal of Geophysical Research: Solid Earth*, *126*(4), e2020JB021125. https://doi.org/10.1029/2020JB021125

Niu, Q. (2023). Revisiting the diffuse layer polarization of a spherical grain in electrolytes with numerical solutions of Nernst-Planck-Poisson equations. *Journal of Geophysical Research: Solid Earth*, *128*(8), e2022JB025934. https://doi.org/10.1029/2022JB025934

Niu, Q., Prasad, M., Revil, A., & Saidian, M. (2016). Textural control on the quadrature conductivity of porous media. *Geophysics*, *81*(5), E297–E309. https://doi.org/10.1190/geo2015-0715.1

Niu, Q., Revil, A., & Saidian, M. (2016). Salinity dependence of the complex surface conductivity of the Portland sandstone. *Geophysics*, *81*(2), D125–D140. https://doi.org/10.1190/geo2015-0426.1

Niu, Q., & Zhang, C. (2017). Pore-scale modelling of complex conductivity of saturated granular materials. *Near Surface Geophysics*, *15*(6), 593–602. https://doi.org/10.3997/1873-0604.2017055

Niwas, S., Gupta, P. K., & de Lima, O. A. (2006). Nonlinear electrical response of saturated shaley sand reservoir and its asymptotic approximations. *Geophysics*, *71*(3), G129–G133. https://doi.org/10.1190/1.2196031

Niwas, S., Gupta, P. K., & De Lima, O. A. L. (2007). Nonlinear electrical conductivity response of shaly-sand reservoir. *Current Science*, 612–617. https://www.jstor.org/stable/24097849

Nordsiek, S., & Weller, A. (2008). A new approach to fitting induced-polarization spectra. *Geophysics*, *73*(6), F235–F245. https://doi.org/10.1190/1.2987412

O'Konski, C. T. (1960). Electric properties of macromolecules. V. Theory of ionic polarization in polyelectrolytes. *The Journal of Physical Chemistry*, *64*(5), 605–619. https://doi.org/10.1021/j100834a023

Palomino, A. M., & Santamarina, J. C. (2005). Fabric map for kaolinite: Effects of pH and ionic concentration on behavior. *Clays and Clay Minerals*, *53*(3), 211–223. https://doi.org/10.1346/CCMN.2005.0530302

Panwar, N., Revil, A., Sharma, R., Schmutz, M., Duvillard, P. A., Garcia, B., et al. (2021). Induced polarization of carbonates. *Journal of Geophysical Research: Solid Earth*, *126*(6), e2021JB022029. https://doi.org/10.1029/2021JB022029

Parsekian, A. D., Singha, K., Minsley, B. J., Holbrook, W. S., & Slater, L. (2015). Multiscale geophysical imaging of the critical zone. *Reviews of Geophysics*, *53*(1), 1–26. https://doi.org/10.1002/2014RG000465

Patnode, H. W., & Wyllie, M. R. J. (1950). The presence of conductive solids in reservoir rocks as a factor in electric log interpretation. *Journal of Petroleum Technology*, *2*(02), 47–52. https://doi.org/10.2118/950047-G

Pelton, W. H., Sill, W. R., & Smith, B. D. (1983). Interpretation of complex resistivity and dielectric data: Part I. *Geophysical Transactions*, *29*(4), 297–330. https://epa.oszk.hu/02900/02941/00057/pdf/

Pelton, W. H., Ward, S. H., Hallof, P. G., Sill, W. R., & Nelson, P. H. (1978). Mineral discrimination and removal of inductive coupling with multifrequency IP. *Geophysics*, *43*(3), 588–609. https://doi.org/10.1190/1.1440839

Peruzzo, L., Liu, X., Chou, C., Blancaflor, E. B., Zhao, H., Ma, X., et al. (2021). Three-channel electrical impedance spectroscopy for field-scale root phenotyping. *The Plant Phenome Journal*, *4*(1), e20021. https://doi.org/10.1002/ppj2.20021

Peruzzo, L., Schmutz, M., Franceschi, M., Wu, Y., & Hubbard, S. S. (2018). The relative importance of saturated silica sand interfacial and pore fluid geochemistry on the spectral induced polarization response. *Journal of Geophysical Research: Biogeosciences*, *123*(5), 1702–1718. https://doi.org/10.1029/2017JG004364

Peshtani, K., Weller, A., Saneiyan, S., & Slater, L. (2022). The influence of magnetic minerals on induced polarization measurements in sedimentary rocks. *Geophysical Research Letters*, *49*(19), e2022GL100192. https://doi.org/10.1029/2022GL100192

Qi, Y., El-Kaliouby, H., Revil, A., Ahmed, A. S., Ghorbani, A., & Li, J. (2019). Three-dimensional modeling of frequency- and time-domain electromagnetic methods with induced polarization effects. *Computers & Geosciences*, *124*, 85–92. https://doi.org/10.1016/j.cageo.2018.12.011

Qi, Y., & Wu, Y. (2022). Electrical conductivity of clayey rocks and soils: A non-linear model. *Geophysical Research Letters*, *49*(10), e2021GL097408. https://doi.org/10.1029/2021GL097408

Qi, Y., & Wu, Y. (2023). Materials for "induced polarization of clayey rocks and soils: Non-linear complex conductivity models" [Dataset]. *Zenodo*. https://doi.org/10.5281/zenodo.10253380

Revil, A. (2013). Effective conductivity and permittivity of unsaturated porous materials in the frequency range 1mHz–1GHz. *Water Resources Research*, *49*(1), 306–327. https://doi.org/10.1029/2012WR012700

Revil, A., Ahmed, A. S., & Matthai, S. (2018). Transport of water and ions in partially water-saturated porous media. Part 3. Electrical conductivity. *Advances in Water Resources*, *121*, 97–111. https://doi.org/10.1016/j.advwatres.2018.08.007

Revil, A., Ghorbani, A., Jougnot, D., & Yven, B. (2023). Induced polarization of clay-rich materials—Part 1: The effect of desiccation. *Geophysics*, *88*(4), MR195–MR210. https://doi.org/10.1190/geo2022-0510.1

Revil, A., Qi, Y., Ghorbani, A., Coperey, A., Ahmed, A. S., Finizola, A., & Ricci, T. (2019). Induced polarization of volcanic rocks. 3. Imaging clay cap properties in geothermal fields. *Geophysical Journal International*, *218*(2), 1398–1427. https://doi.org/10.1093/gji/ggz207

Revil, A., & Skold, M. (2011). Salinity dependence of spectral induced polarization in sands and sandstones. *Geophysical Journal International*, *187*(2), 813–824. https://doi.org/10.1111/j.1365-246X.2011.05181.x

Rink, M., & Schopper, J. R. (1974). Interface conductivity and its implications to electric logging. In *SPWLA 15th annual logging symposium*.

Robinson, D. A., Binley, A., Crook, N., Day-Lewis, F. D., Ferré, T. P. A., Grauch, V. J. S., et al. (2008). Advancing process-based watershed hydrological research using near-surface geophysics: A vision for, and review of, electrical and magnetic geophysical methods. *Hydrological Processes*, *22*(18), 3604–3635. https://doi.org/10.1002/hyp.6963

Rubin, Y., & Hubbard, S. S. (Eds.) (2006). *Hydrogeophysics* (Vol. 50). Springer.

Saneiyan, S., Ntarlagiannis, D., & Colwell, F. (2021). Complex conductivity signatures of microbial induced calcite precipitation, field and laboratory scales. *Geophysical Journal International*, *224*(3), 1811–1824. https://doi.org/10.1093/gji/ggaa510

Saner, S., & Akbar, M. (2010). Excess electrical conductance in carbonate rocks. In *Paper SCA2010-28, proceeding of the international symposium of the society of core analysts*. Retrieved from https://www.jgmaas.com/SCA/2010/SCA2010-28.pdf

Schlumberger, C. (1920). *Study of underground electrical prospecting*. Gauthier-Villars.

Schmutz, M., Blondel, A., & Revil, A. (2012). Saturation dependence of the quadrature conductivity of oil-bearing sands. *Geophysical Research Letters*, *39*(3), L03402. https://doi.org/10.1029/2011GL050474

Schön, J. H. (2015). *Physical properties of rocks: Fundamentals and principles of petrophysics*. Elsevier.

Schroeder, P. A. (2018). *Clays in the critical zone*. Cambridge University Press.

Schurr, J. M. (1964). On the theory of the dielectric dispersion of spherical colloidal particles in electrolyte solution. *The Journal of Physical Chemistry*, *68*(9), 2407–2413. https://doi.org/10.1021/j100791a004
Schwarz, G. (1962). A theory of the low-frequency dielectric dispersion of colloidal particles in electrolyte solution. *The Journal of Physical Chemistry*, *66*(12), 2636–2642. https://doi.org/10.1021/j100818a067
Seigel, H., Nabighian, M., Parasnis, D. S., & Vozoff, K. (2007). The early history of the induced polarization method. *The Leading Edge*, *26*(3), 312–321. https://doi.org/10.1190/1.2715054
Sen, P. N., Scala, C., & Cohen, M. H. (1981). A self-similar model for sedimentary rocks with application to the dielectric constant of fused glass beads. *Geophysics*, *46*(5), 781–795. https://doi.org/10.1190/1.1441215
Shuey, R. T., & Johnson, M. (1973). On the phenomenology of electrical relaxation in rocks. *Geophysics*, *38*(1), 37–48. https://doi.org/10.1190/1.1440331
Sihvola, A. (1999). *Electromagnetic mixing formulas and applications*. IET.
Skold, M., Revil, A., & Vaudelet, P. (2011). The pH dependence of spectral induced polarization of silica sands: Experiment and modeling. *Geophysical Research Letters*, *38*(12), L12304. https://doi.org/10.1029/2011GL047748
Slater, L. (2007). Near surface electrical characterization of hydraulic conductivity: From petrophysical properties to aquifer geometries—A review. *Surveys in Geophysics*, *28*(2), 169–197. https://doi.org/10.1007/s10712-007-9022-y
Slater, L. D., & Glaser, D. R. (2003). Controls on induced polarization in sandy unconsolidated sediments and application to aquifer characterization. *Geophysics*, *68*(5), 1547–1558. https://doi.org/10.1190/1.1620628
Slater, L. D., & Lesmes, D. (2002). IP interpretation in environmental investigations. *Geophysics*, *67*(1), 77–88. https://doi.org/10.1190/1.1451353
Soininen, H. (1984). The behavior of the apparent resistivity phase spectrum in the case of a polarizable prism in an unpolarizable half-space. *Geophysics*, *49*(9), 1534–1540. https://doi.org/10.1190/1.1441778
Song, Y., Shi, X., Revil, A., & Kang, X. (2022). Monitoring in situ microbial growth and decay in soil column experiments by induced polarization. *Geophysical Research Letters*, *49*(16), e2021GL097553. https://doi.org/10.1029/2021GL097553
Šumi, F. (1965). Prospecting for non-metallic minerals by induced polarization. *Geophysical Prospecting*, *13*(4), 603–616. https://doi.org/10.1111/j.1365-2478.1965.tb01952.x
Sumner, J. S. (1976). *Principles of induced polarization for geophysical exploration*. Elsevier.
Tabbagh, A., Rejiba, F., Finco, C., Schamper, C., Souffaché, B., Camerlynck, C., et al. (2021). The case for considering polarization in the interpretation of electrical and electromagnetic measurements in the 3 kHz to 3 MHz frequency range. *Surveys in Geophysics*, *42*(2), 377–397. https://doi.org/10.1007/s10712-020-09625-1
Tarasov, A., & Titov, K. (2013). On the use of the Cole–Cole equations in spectral induced polarization. *Geophysical Journal International*, *195*(1), 352–356. https://doi.org/10.1093/gji/ggt251
Tournassat, C., Grangeon, S., Leroy, P., & Giffaut, E. (2013). Modeling specific pH dependent sorption of divalent metals on montmorillonite surfaces. A review of pitfalls, recent achievements and current challenges. *American Journal of Science*, *313*(5), 395–451. https://doi.org/10.2475/05.2013.01
Tournassat, C., Steefel, C. I., Bourg, I. C., & Bergaya, F. (2015). *Natural and engineered clay barriers*. Elsevier.
Tsukanov, K., & Schwartz, N. (2021). Modeling plant roots spectral induced polarization signature. *Geophysical Research Letters*, *48*(5), e2020GL090184. https://doi.org/10.1029/2020GL090184
Vinegar, H. J., & Waxman, M. H. (1984). Induced polarization of shaly sands. *Geophysics*, *49*(8), 1267–1287. https://doi.org/10.1190/1.1441755
Wang, C., & Slater, L. D. (2019). Extending accurate spectral induced polarization measurements into the kHz range: Modelling and removal of errors from interactions between the parasitic capacitive coupling and the sample holder. *Geophysical Journal International*, *218*(2), 895–912. https://doi.org/10.1093/gji/ggz199
Waxman, M. H., & Smits, L. J. M. (1968). Electrical conductivities in oil-bearing shaly sands. *Society of Petroleum Engineers Journal*, *8*(02), 107–122. https://doi.org/10.2118/1863-A
Weigand, M., & Kemna, A. (2016a). Debye decomposition of time-lapse spectral induced polarisation data. *Computers & Geosciences*, *86*, 34–45. https://doi.org/10.1016/j.cageo.2015.09.021
Weigand, M., & Kemna, A. (2016b). Relationship between Cole–Cole model parameters and spectral decomposition parameters derived from SIP data. *Geophysical Journal International*, *205*(3), 1414–1419. https://doi.org/10.1093/gji/ggw099
Weller, A., & Slater, L. (2012). Salinity dependence of complex conductivity of unconsolidated and consolidated materials: Comparisons with electrical double layer models. *Geophysics*, *77*(5), D185–D198. https://doi.org/10.1190/geo2012-0030.1
Weller, A., & Slater, L. (2019). Permeability estimation from induced polarization: An evaluation of geophysical length scales using an effective hydraulic radius concept. *Near Surface Geophysics*, *17*(6), 581–594. https://doi.org/10.1002/nsg.12071
Weller, A., & Slater, L. (2022). Ambiguity in induced polarization time constants and the advantage of the Pelton model. *Geophysics*, *87*(6), E393–E399. https://doi.org/10.1190/geo2022-0158.1
Weller, A., Slater, L., Huisman, J. A., Esser, O., & Haegel, F. H. (2015). On the specific polarizability of sands and sand-clay mixtures. *Geophysics*, *80*(3), A57–A61. https://doi.org/10.1190/geo2014-0509.1
Weller, A., Slater, L., & Nordsiek, S. (2013). On the relationship between induced polarization and surface conductivity: Implications for petrophysical interpretation of electrical measurements. *Geophysics*, *78*(5), D315–D325. https://doi.org/10.1190/geo2013-0076.1
Weller, A., Slater, L., Nordsiek, S., & Ntarlagiannis, D. (2010). On the estimation of specific surface per unit pore volume from induced polarization: A robust empirical relation fits multiple data sets. *Geophysics*, *75*(4), WA105–WA112. https://doi.org/10.1190/1.3471577
Weller, A., Zhang, Z., & Slater, L. (2015). High-salinity polarization of sandstones. *Geophysics*, *80*(3), D309–D318. https://doi.org/10.1190/geo2014-0483.1
Winsauer, W. O., & McCardell, W. M. (1953). Ionic double-layer conductivity in reservoir rock. *Journal of Petroleum Technology*, *5*(05), 129–134. https://doi.org/10.2118/953129-G
Worthington, P. F. (1985). The evolution of shaly-sand concepts in reservoir evaluation. *Log Analyst*, *26*(01). SPWLA-1985-vXXVIn1a2.
Wu, Y., Ajo-Franklin, J. B., Spycher, N., Hubbard, S. S., Zhang, G., Williams, K. H., et al. (2011). Geophysical monitoring and reactive transport modeling of ureolytically-driven calcium carbonate precipitation. *Geochemical Transactions*, *12*(1), 1–20. https://doi.org/10.1186/1467-4866-12-7
Wu, Y., Hubbard, S., Williams, K. H., & Ajo-Franklin, J. (2010). On the complex conductivity signatures of calcite precipitation. *Journal of Geophysical Research*, *115*(G2), G00G04. https://doi.org/10.1029/2009JG001129
Wyllie, M. R. J., & Southwick, P. F. (1954). An experimental investigation of the SP and resistivity phenomena in dirty sands. *Journal of Petroleum Technology*, *6*(02), 44–57. https://doi.org/10.2118/302-G

Zhang, C., Revil, A., Fujita, Y., Munakata-Marr, J., & Redden, G. (2014). Quadrature conductivity: A quantitative indicator of bacterial abundance in porous media. *Geophysics*, *79*(6), D363–D375. https://doi.org/10.1190/geo2014-0107.1

Zhdanov, M. S., & Fang, S. (1996). Quasi-linear approximation in 3-D electromagnetic modeling. *Geophysics*, *61*(3), 646–665. https://doi.org/10.1190/1.1443994

Zimmermann, E., & Huisman, J. A. (2024). The effect of heterogeneous contact impedances on complex resistivity measurements. *Geophysical Journal International*, *236*(3), 1234–1245. https://doi.org/10.1093/gji/ggad477

Zimmermann, E., Kemna, A., Berwix, J., Glaas, W., Münch, H. M., & Huisman, J. A. (2008). A high-accuracy impedance spectrometer for measuring sediments with low polarizability. *Measurement Science and Technology*, *19*(10), 105603. https://doi.org/10.1088/0957-0233/19/10/105603

References From the Supporting Information

Balanis, C. A. (1989). *Advanced engineering electromagnetics*. Wiley.

Ingeman-Nielsen, T., & Baumgartner, F. (2006). Numerical modelling of complex resistivity effects on a homogenous half-space at low frequencies. *Geophysical Prospecting*, *54*(3), 261–271. https://doi.org/10.1111/j.1365-2478.2006.00532.x

Kemna, A. (2000). *Tomographic inversion of complex resistivity: Theory and application*. Der Andere Verlag.

Kong, J. A. (1986). *Electromagnetic wave theory*. Wiley.

Weigand, M., Zimmermann, E., Michels, V., Huisman, J. A., & Kemna, A. (2022). Design and operation of a long-term monitoring system for spectral electrical impedance tomography (sEIT). *Geoscientific Instrumentation, Methods and Data Systems*, *11*(2), 413–433. https://doi.org/10.5194/gi-11-413-2022